J|A|C|S
ARTICLES

Molecular Silicate and Aluminate Species in Anhydrous and Hydrated Cements

Aditya Rawal,[†] Benjamin J. Smith,[†] George L. Athens,[†] Christopher L. Edwards,[‡] Lawrence Roberts,[§] Vijay Gupta,[ǁ] and Bradley F. Chmelka*,[†]

Department of Chemical Engineering, University of California, Santa Barbara, California 93106, Halliburton, Duncan, Oklahoma 73533, Roberts Consulting Group, 44 Windsor Avenue, Acton, Massachusetts 01720, and RTI International, Research Triangle Park, North Carolina 27709

Received September 24, 2009; E-mail: bradc@engineering.ucsb.edu

Abstract: The compositions and molecular structures of anhydrous and hydrated cements are established by using advanced solid-state nuclear magnetic resonance (NMR) spectroscopy methods to distinguish among different molecular species and changes that occur as a result of cement hydration and setting. One- and two-dimensional (2D) solid-state ^{29}Si and ^{27}Al magic-angle spinning NMR methodologies, including T_1-relaxation-time- and chemical-shift-anisotropy-filtered measurements and the use of very high magnetic fields (19 T), allow resonances from different silicate and aluminate moieties to be resolved and assigned in complicated spectra. Single-pulse ^{29}Si and ^{27}Al NMR spectra are correlated with X-ray fluorescence results to quantify the different crystalline and disordered silicate and aluminate species in anhydrous and hydrated cements. 2D $^{29}Si\{^1H\}$ and $^{27}Al\{^1H\}$ heteronuclear correlation NMR spectra of hydrated cements establish interactions between water and hydroxyl moieties with distinct ^{27}Al and ^{29}Si species. The use of a ^{29}Si T_1-filter allows anhydrous and hydrated silicate species associated with iron-containing components in the cements to be distinguished, showing that they segregate from calcium silicate and aluminate components during hydration. The different compositions of white Portland and gray oilwell cements are shown to have distinct molecular characteristics that are correlated with their hydration behaviors.

Introduction

Cement as a material of construction has been in use since ancient times, evolving from the Egyptian civilization[1] and with building examples from the Romans standing to this day.[2] Portland cement was formulated and patented[3] in 1824 and has since become one of the most extensively used engineering materials, primarily as the major component of concrete. Portland cement is formed by blending, grinding, and heating raw materials, principally limestone and clays, together at 1300−1500 °C to form so-called cement "clinker", which is interground with up to 5% calcium sulfate dihydrate ($CaSO_4 \cdot 2H_2O$, gypsum) to produce cement. The anhydrous cement is a complicated solid mixture of a number of components that vary in concentration, depending on the raw materials and cement kiln conditions used in its preparation, and these components impact the properties of the cement differently. Portland cements generally contain 50−70 wt % Ca_3SiO_5, 5−25 wt % Ca_2SiO_4, 0−15 wt % $Ca_3Al_2O_6$, and 0−15 wt % aluminoferrite ($Ca_2Al_xFe_{2-x}O_5$; 0 < x < 1.4).[4,5] Ca_3SiO_5 (trical-

cium silicate, often called "alite", or denoted in cement chemists' shorthand as C₃S, where "C" stands for CaO, and "S" stands for SiO_2) and its polymorphs react quickly with water, making these silicate phases primarily responsible for early setting and strength development of hydrated cements.[6] Ca_2SiO_4 (dicalcium silicate or $2CaO \cdot SiO_2$ often called "belite," or denoted as C₂S) and its polymorphs are responsible for the development of mechanical strength over longer time scales (ca. months to years), as they react with water more slowly.[6] Among the different aluminate phases, $Ca_3Al_2O_6$ (tricalcium aluminate or $3CaO \cdot Al_2O_3$, denoted as C₃A, where "A" stands for Al_2O_3) and aluminoferrite (a nonstoichiometric tetracalcium aluminate denoted as C₄AF, where "F" stands for Fe_2O_3) are typically present in varying extents. Surface aluminate species react with water, often relatively rapidly within the first 30 min of hydration, which can cause undesirable "flash" setting of cements that can result in loss of plasticity and poor strength development.[6] There exist numerous other ions, such as Na^+, Mg^{2+}, K^+, Fe^{3+}, SO_4^{2-}, and PO_4^{3-}, that are present either as substituents of the main components or form small amounts of separate silicate or alkali phases themselves. Many cements acquire their characteristic gray color from iron in the alumi-noferrite phases that often complicate molecular analyses of their properties by nuclear magnetic resonance (NMR) spectroscopy. Cements with low iron contents (<0.5 wt %)[7] tend to be white

[†] University of California.
[‡] Halliburton.
[§] Roberts Consulting Group.
[ǁ] RTI International.
(1) Gadalla, M. *Pyramid Illusions*; Bastet Publishing: Erie, PA, 1997.
(2) Sharp, J. H. *Adv. Appl. Ceram.* **2006**, *105*, 162−174.
(3) Aspdin, J. British Patent 5022, 1824.
(4) Skibsted, J.; Jakobsen, H. J.; Hall, C. *J. Chem. Soc., Faraday Trans.* **1994**, *90*, 2095−2098.
(5) Skibsted, J.; Jakobsen, H. J.; Hall, C. *Adv. Cem. Based Mater.* **1998**, *7*, 57−59.

(6) Taylor, H. F. W. *Cement Chemistry*; Academic Press: London, 1990.
(7) Hamad, B. S. *Adv. Cem. Based Mater.* **1995**, *2*, 161−167.

in color and have often been used in scientific studies to avoid the complicating effects of the iron components on characterization.

A variety of additives may be used to modify both the hydration behaviors of the initially anhydrous cement mixtures or the final properties of the hydrated cements. For example, calcium sulfate is generally added to moderate the fast reactions of aluminates with water, thereby reducing the tendency of the cement to "flash set" and aiding the development of desirable mechanical properties. The reaction of tricalcium aluminate (C_3A) with water and calcium sulfate forms the mineral ettringite (hexacalcium aluminate trisulfate hydrate $(CaO)_6(Al_2O_3)(SO_3)_3 \cdot 32H_2O$) on the surfaces of C_3A, which slows cement setting.[8] In the case of high iron contents (which are typical of oilwell cements), inadequate sulfate concentrations can also result in slow setting. In general, the relative concentrations of the different components in anhydrous cements affect the viscoelasticity, setting, and mechanical properties of hydrating cements in complicated and interrelated ways.[9]

Despite cement's extensive history of use, the molecular compositions, structures, and changes that occur as a result of hydration (i.e., setting) remain poorly understood. In part, this has been due to challenges associated with the characterization of such complicated multicomponent, heterogeneous, and non-equilibrium solid-state materials and processes, in which reacting interfaces between different components play large roles. These issues are general to a wide variety of heterogeneous inorganic solids and mixtures within the chemical sciences. For silicate, aluminate, aluminosilicate, and silica−alumina materials similar to cements, complex hydration behaviors are important to the syntheses, structures, and resulting properties of ceramics,[10,11] zeolite catalysts,[12−14] mesoporous materials,[15,16] sol−gel-derived glasses,[17,18] and biominerals.[19−23] These complicated chemical systems share common challenges to measure, identify, and control the evolution of precursor components as they are converted to heterogeneous solid products.

Cements represent a particularly complex class of materials because of their multiphase character before, during, and after hydration. Diverse methods have been used to characterize cement composition and structure, including X-ray diffraction (XRD) for analyses of crystalline phases in both anhydrous and hydrated cements, infrared and Raman spectroscopies for detection of both amorphous and crystalline components, and more recently, X-ray absorption spectroscopy to identify distributions of minor elements on a length scale of several micrometers.[24] In particular, Rietveld refinements of wide-angle XRD data have been used extensively to identify and characterize the crystalline phases present in cement clinker.[24] However, insights from XRD on noncrystalline, heavily defected, or surface species that lack long-range order are generally limited, though these feature prominently in both anhydrous and hydrated cements.

Advanced NMR spectroscopy techniques are sensitive to local chemical compositions and structures in solid- and solution-state materials, including those without long-range order. The information provided therefore augments that obtained from scattering, vibrational spectroscopy, or bulk property measurements, which probe complementary length scales and processes.[25,26] The selectivity of NMR, furthermore, enables the detection and monitoring of cement species containing NMR-active isotopes of different elements, such as ^1H, ^{27}Al, and ^{29}Si, which can be independently measured and correlated. One-dimensional (1D) single-pulse NMR measurements are generally quantitative, allowing resolved species to be evaluated and their relative populations monitored over time, as the cement hydrates and solidifies. 1D single-pulse ^{29}Si NMR has been used extensively to characterize the silicate species in anhydrous and hydrated cement pastes,[24,27,28] from which it has been established that the primary silicate constituents of cements are so-called Q^0 ^{29}Si silicate species that compose tri- and dicalcium silicate (C_3S and C_2S) phases. ("Q^n" refers to ^{29}Si atoms that are covalently bonded via bridging oxygen atoms to $n \leq 4$ other Si atoms;[29] "$Q^n(mAl)$" similarly refers to a ^{29}Si atom bonded via bridging oxygen atoms to n other silicon or aluminum atoms, m of which are Al.) During the hydration process, more condensed silicate species form disordered products, such as calcium-silicate-hydrates (often denoted as C-S-H, and hereafter referred to as "CSH" for brevity), which are characterized by Q^1 and Q^2 ^{29}Si moieties with broad distributions of local environments[24] that are typically not resolved by single-pulse ^{29}Si MAS NMR or other methods. In cements hydrated for longer times, Q^3 and Q^4 ^{29}Si silicate species are also prevalent, which indicates a more densely cross-linked silicate network, as expected.

Similarly, solid-state 1D ^{27}Al NMR measurements have shown that aluminate species in anhydrous Portland cement have principally 4-fold coordination (Al^{IV}), a significant fraction of which is converted upon hydration into five-coordinate Al^V, six-coordinate Al^{VI}, and different Al^{IV} species.[4,30] The primary aluminate (C_3A) and aluminoferrite (C_4AF) phases in anhydrous cements are composed principally of Al^{IV} species whose ^{27}Al NMR signals are often extensively broadened by ferro- or paramagnetic iron components in close proximity.[5] These iron

(8) Meredith, P.; Donald, A. M.; Meller, N.; Hall, C. *J. Mater. Sci.* **2004**, *39*, 997–1005.
(9) Jons, E. S.; Osbaeck, B. *Cem. Concr. Res.* **1982**, *12*, 167–78.
(10) Sigmund, W. M.; Bell, N. S.; Bergström, L. *J. Am. Ceram. Soc.* **2000**, *83*, 1557–1574.
(11) Bill, J.; Aldinger, F. *Adv. Mater.* **1995**, *7*, 775.
(12) Lee, Y.; Vogt, T.; Hriljac, J. A.; Parise, J. B.; Hanson, J. C.; Kim, S. J. *Nature* **2002**, *420*, 485–489.
(13) Hass, K. C.; Schneider, W. F.; Curioni, A.; Andreoni, W. *Science* **1998**, *282*, 882–882.
(14) Corma, A. *J. Catal.* **2003**, *216*, 298–312.
(15) Taguchi, A.; Schüth, F. *Microporous Mesoporous Mater.* **2005**, *77*, 1–45.
(16) Ying, J. Y.; Mehnert, C. P.; Wong, M. S. *Angew. Chem., Int. Ed.* **1999**, *38*, 56–77.
(17) Baccile, N.; Babonneau, F.; Thomas, B.; Coradin, T. *J. Mater. Chem.* **2009**, *19*, 8537–8559.
(18) Livage, J. *Curr. Opin. Solid State Mater. Sci.* **1997**, *2*, 132–138.
(19) Aizenberg, J.; Weaver, J. C.; Thanawala, M. S.; Sundar, V. C.; Morse, D. E.; Fratzl, P. *Science* **2005**, *309*, 275–278.
(20) Heuer, A. H.; Fink, D. J.; Laraia, V. J.; Arias, J. L.; Calvert, P. D.; Kendall, K.; Messing, G. L.; Blackwell, J.; Rieke, P. C.; Thompson, D. H.; Wheeler, A. P.; Veis, A.; Caplan, A. I. *Science* **1992**, *255*, 1098–1105.
(21) Pietak, A. M.; Reid, J. W.; Stott, M. J.; Sayer, M. *Biomaterials* **2007**, *28*, 4023–4032.
(22) Komnitsas, K.; Zaharaki, D. *Miner. Eng.* **2007**, *20*, 1261–1277.
(23) Brown, G. E. *Science* **2001**, *294*, 67–69.

(24) Skibsted, J.; Hall, C. *Cem. Concr. Res.* **2008**, *38*, 205–225.
(25) Colombet, P. *Nuclear Magnetic Resonance Spectroscopy of Cement-Based Materials*: Springer-Verlag: Berlin, 1999; Vol. 37.
(26) Skibsted, J.; Hall, C.; Jakobsen, H. J. In *Structure and Performance of Cements*; Bensted, J., Barnes, P., Eds.; Spon Press: New York, 2002.
(27) Zanni, H.; Rassem-Bertolo, R.; Masse, S.; Fernandez, L.; Nieto, P.; Bresson, B. *Magn. Reson. Imag.* **1996**, *14*, 827–831.
(28) Edwards, C. L.; Alemany, L. B.; Barron, A. R. *Ind. Eng. Chem. Res.* **2007**, *46*, 5122–5130.
(29) Engelhardt, G.; Michel, D. *High-Resolution Solid-State NMR of Silicates and Zeolites*; John Wiley & Sons: Chichester, 1987.
(30) Le Saout, G.; Lecolier, E.; Rivereau, A.; Zanni, H. *Cem. Concr. Res.* **2006**, *36*, 428–433.

components can be present in crystalline or disordered regions as cations, oxides, and/or hydroxides (e.g., Fe^{2+}, Fe^{3+}, Fe_2O_3, Fe_3O_4, $Fe(OH)_3$, referred to broadly as "ferrites" within the cement literature) with indefinite compositions and distributions.[6] During hydration, Al^{IV} and Al^V aluminate species are thought to react with the calcium silicate species and be partially incorporated into the CSH, with some Al^{IV} species replacing four-coordinated ^{29}Si atoms, while the Al^V species form in the interlayers of the CSH gel.[31] The Al^{VI} species are primarily thought to be associated with hydrated tricalcium aluminate and aluminoferrite phases ($[Ca_2(Al,Fe)(OH)_6] \cdot X \cdot xH_2O$ (often denoted "AFm") or $[Ca_3Al_yFe_{1-y}(OH)_6 \cdot 12H_2O]_2 \cdot X_3 \cdot xH_2O$ (denoted "AFt"), where X represents an anion.[5] Additional aluminate hydrate products, such as the so-called "third aluminate hydrate" (TAH), are also thought to form,[32] though their molecular compositions, structures, and interactions during hydration are not well understood. 1D single-pulse ^{27}Al NMR has been used to identify and quantify the substitution of Al atoms in the di- and tricalcium silicate (C_2S, C_3S) phases of both white Portland and oilwell cements.[4] Similar single-pulse ^{27}Al NMR spectra of synthetic calcium aluminoferrites showed no resolved ^{27}Al signals (at 9.4 T), most likely due to the presence of the para/ferromagnetic iron-containing components.[5] 1D single-pulse ^{27}Al NMR measurements of hydrated Portland and oilwell cements[30] revealed the presence of broad distributions of Al^{IV}, Al^V, and Al^{VI} species that are thought to be incorporated into the CSH or hydrated aluminate products, although signals from distinct species were not resolved.

Powerful two-dimensional (2D) NMR spectroscopy techniques provide significantly enhanced spectral resolution that allows different molecular species in complicated cement mixtures to be identified and their mutual interactions and molecular proximities established. For example, $^{29}Si\{^{29}Si\}$ homonuclear and $^{29}Si\{^1H\}$ heteronuclear correlation NMR techniques have been used to investigate ^{29}Si-enriched CSH and show that, at low Ca/Si ratios (0.7−1.5), water molecules are in close proximities to ^{29}Si, while higher Ca/Si ratios lead to increased concentrations of CaOH-type protons.[33] 2D $^1H\{^1H\}$ correlation NMR has been used to investigate hydrated cements with organic modifiers, such as methyl cellulose, that are added to stabilize cement suspensions.[34] The amorphous CSH hydration product(s) are thought to play a key role in the development, cohesion, and durability of hydrated Portland cement,[33] although much remains unknown about its local chemical compositions and structures. The heterogeneous molecular environments of bulk and surface silicate, aluminate, and proton species in cement, their interactions, and chemical transformations during hydration remain inadequately characterized.

In several studies, molecular NMR measurements of cements have relied on laboratory-synthesized components with high purities and high crystallinities.[33,35] This reduces complications from distributions of metal-ion substituents, such as Mg^{2+}, Al^{3+}, or Fe^{3+}, and accompanying variations in polymorphism of the different components, yielding NMR spectra with improved

resolution and sensitivity. Laboratory-synthesized compounds also have the advantage that they can be isotopically enriched (e.g., in ^{29}Si) to enhance the sensitivity of the measurements.[33] However, the chemical and structural transformations that occur during hydration of these model systems may differ from those observed in the multicomponent, nonequilibrium, and disordered cement systems used industrially.

Here, the complex heterogeneous molecular compositions and structures of anhydrous and hydrated cements are analyzed by advanced solid-state NMR techniques that establish and monitor the molecular-level changes that occur during hydration. Specifically, different molecular silicate and aluminate species in anhydrous and hydrated white Portland and gray oilwell cements are resolved, identified, and quantified using a combination of powerful 1D and 2D solid-state ^{29}Si and ^{27}Al NMR methods, in conjunction with X-ray fluorescence, X-ray diffraction, and scanning electron microscopy. Molecular interactions between ^{27}Al or ^{29}Si species and water or hydroxyl groups in the hydrated cements are elucidated, providing new insights on the heterogeneous molecular processes that occur during setting. This is expected to have important implications for understanding the conditions, chemical compositions, and molecular structures associated with cement setting and the mechanical properties of hydrated cements and other mixed oxide materials.

Experimental Section

Anhydrous Aalborg white Portland cement (WPC, Lehigh Cement) and API Class H gray oilwell cement (GOC, Lafarge) were used as received. Hydrated cement pastes were prepared by mixing the anhydrous cements with water in a high shear blender (Waring, Model HGB2WTG4) at ca. 10,000 rpm for 1 min. Water-to-cement mass ratios of 0.44 and 0.38 were used for the WPC and GOC, respectively, which are typical of industrial formulations and differed due to differing water requirements of the two cements to yield stable pastes. The slurries were then poured into polyethylene containers and hydrated at room temperature and 100% relative humidity. After 4 weeks, the hydrated cement pastes were immersed in liquid nitrogen to quench the hydration reaction and subsequently ground into powders, while immersed in liquid nitrogen. The frozen powder samples were then placed under vacuum at 0.10 Torr to remove unreacted water by freeze-drying at 233 K. This method was used, instead of quenching in an acetone bath,[33] to avoid the inclusion of extraneous organic moieties in the hydrated cements. The freeze-dried cements were stored in sealed vessels under vacuum and monitored over a period of one year by solid-state ^{29}Si, ^{27}Al, and ^1H NMR spectroscopy to ensure that there were no molecular-level changes in the samples, such as might occur because of adsorption of moisture or reaction with CO_2 from the atmosphere.

XRD patterns were acquired on a Philips XPERT powder diffractometer using Cu K_α radiation with a wavelength of 0.154 nm. The samples were scanned at 0.9°/min between 2θ angles of 10−70° for white Portland cement (Supporting Information, Figure S1) and 20−70° for gray oilwell cement (Supporting Information, Figure S2). X-ray fluorescence analyses were performed to determine the elemental compositions of the white Portland and gray oilwell cements. A variety of elements were detected and their relative bulk weight percentages are listed in Table 1.

Scanning electron micrographs were conducted using a FEI XL30 Sirion FEG digital electron scanning microscope at a magnification of 2000× for anhydrous white Portland cement (Supporting Information, Figure S3A) and 10000× for hydrated white Portland cement (Supporting Information, Figure S3B). Compressive strength measurements were performed on the hydrated solid cements using an Instron 1123 displacement-controlled compression tester with a constant downward velocity of 0.2 mm/min. Ten cylindrical test

(31) Sun, G. K.; Young, J. F.; Kirkpatrick, R. J. *Cem. Concr. Res.* **2006**, *36*, 18–29.

(32) Andersen, M. D.; Jakobsen, H. J.; Skibsted, J. *Cem. Concr. Res.* **2006**, *36*, 3–17.

(33) Brunet, F.; Bertani, P.; Charpentier, T.; Nonat, A.; Virlet, J. *J. Phys. Chem. B* **2004**, *108*, 15494–15502.

(34) Rottstegge, J.; Wilhelm, M.; Spiess, H. W. *Cem. Concr. Comp.* **2006**, *28*, 417–426.

(35) Faucon, P.; Charpentier, T.; Bertrandie, D.; Nonat, A.; Virlet, J.; Petit, J. C. *Inorg. Chem.* **1998**, *37*, 3726–3733.

Table 1. X-ray Fluorescence Elemental Analyses (Expressed as Oxides) of the Anhydrous White Portland and Gray Oilwell Cements Used in This Study

analyte	white Portland cement (wt %)	gray oilwell cement (wt %)
SiO_2	24.0	20.9
Al_2O_3	2.0	3.0
Fe_2O_3	0.35	4.3
CaO	67.0	63.5
MgO	0.58	3.3
SO_3	2.0	2.8
Na_2O	0.17	0.09
K_2O	0.05	0.27
TiO_2	0.08	0.19
P_2O_5	0.37	0.09
Mn_2O_3	0.02	0.06
SrO	0.13	0.10
Cr_2O_3	<0.01	0.02
ZnO	<0.01	0.03
L.O.I.[a] (950 °C)	1.9	1.0
Total	98.65	99.65

[a] Loss On Ignition: material that volatizes upon heating to 950 °C.

specimens each with a diameter of 15.75 mm and height of 15.75 mm were measured for both white Portland and gray oilwell cements.

Solid-state NMR spectroscopy was used to characterize the molecular compositions and structures of anhydrous and hydrated white Portland and gray oilwell cements. The types of information provided by the different NMR techniques used are summarized in the Supporting Information, Table S1. Solid-state 1D single-pulse ^{1}H, [29]Si, and [27]Al magic-angle spinning (MAS), [29]Si{[1]H} and [27]Al{[1]H} cross-polarization (CP) MAS, [29]Si T_1-filtered, [29]Si chemical-shift-anisotropy (CSA)-filtered, [29]Si{[1]H} Rotational-Echo DOuble-Resonance (REDOR), and 2D [29]Si{[1]H} and [27]Al{[1]H} HETeronuclear CORrelation (HETCOR) NMR experiments were conducted on a Bruker AVANCE-II NMR spectrometer, with an 11.7 T wide-bore superconducting magnet, operating at frequencies of 500.24 MHz for ^{1}H, 99.38 MHz for [29]Si, and 130.35 MHz for [27]Al. (The natural abundances of "NMR-active" [1]H and [27]Al are 100%, while [29]Si is 4.7%.) The measurements were performed under conditions of 5 kHz MAS using a Bruker 7 mm H-X double-resonance MAS probehead with variable-temperature capabilities and zirconia rotors with Kel-F caps. 1D single-pulse [29]Si MAS experiments were conducted on the white Portland cements using a 90° pulse length of 4.0 μs for [29]Si, under conditions of proton decoupling (2.5 μs 90° [1]H pulses, 4.0 dB), with a recycle delay of 60 s. Analogous 1D single-pulse [29]Si MAS experiments were conducted on the gray oilwell cements using a 90° pulse length of 3.6 μs for [29]Si, under conditions of proton decoupling (2.5 μs 90° [1]H pulses, 4.0 dB), with a recycle delay of 10 s. Quantitative single-pulse [29]Si MAS measurements were calibrated using 188 mg of tetrakis(trimethyl-silyl)silane (TKS) as an external reference for [29]Si spin counting, which was measured using 90° pulse lengths of 3.6 μs for [29]Si under conditions of proton decoupling (2.5 μs 90° [1]H pulses, 4.0 dB), with a recycle delay of 1800 s. (The long T_1 reflects the high degree of crystallinity of the TKS sample.)

[29]Si spin—lattice relaxation-time behaviors of the cements were established by using complementary 1D saturation-recovery and T_1-filtered [29]Si MAS spectra, which were used to measure fast- and slow-relaxing species, respectively. 1D saturation-recovery [29]Si MAS spectra were acquired to assess fast-relaxing [29]Si species in gray cements relative to a range of times, τ, between 1 μs and 3 s. The saturation-recovery measurements were performed under conditions of 10 kHz MAS without high-power ^{1}H decoupling, using 90° pulse lengths of 3.6 μs for [29]Si, a 400-pulse saturation train, with 2 μs between saturation pulses, and a 1 ms recycle delay. T_1 values have been previously reported to be ~1 s and ~0.2 s for [29]Si species in the C_2S and C_3S phases of gray oilwell cement,

respectively.[28,36] 1D T_1-filtered [29]Si MAS spectra were acquired with two consecutive [29]Si 90° pulses, followed by a time delay, t_{T1} = 10 s for white Portland cement or t_{T1} = 2 s for gray oilwell cement, and then another [29]Si 90° pulse before detection to suppress [29]Si signals from species with spin—lattice relaxation times shorter than the respective t_{T1} values. Otherwise identical conditions were used as for the 1D single-pulse measurements (i.e., [29]Si, [1]H 90° pulse lengths, proton decoupling) for both white Portland and gray oilwell cement. The 1D T_1-filtered [29]Si MAS spectra were scaled using an appropriate constant $c > 1$ to account for decreased signal intensity due to T_1 relaxation effects that allow remaining signals to be normalized for comparison with the single-pulse [29]Si spectra.

1D CSA-filtered [29]Si MAS spectra were acquired using a five-pulse CSA-filter sequence with a z-filter and TOtal-Suppression-of-Sidebands (TOSS)[37] at 5 kHz MAS, with identical pulse lengths as for the single-pulse [29]Si measurements and with a short (1 μs) or long (43 μs) recoupling time, t_{csa}, included prior to detection. 1D [29]Si{[1]H} REDOR spectra were acquired using two [1]H 180° recoupling pulses per rotor period,[38] a 10 s recycle delay, and different [1]H—[29]Si dipolar recoupling times, t_{rec}, of 0.4 ms, 2.4 and 10.4 ms; the REDOR measurements were corrected for [29]Si T_2 relaxation during recoupling. 1D single-pulse [27]Al MAS spectra were acquired using a high power 1 μs pulse, corresponding to a tip angle of 30° and a recycle delay of 0.5 s. 1D [29]Si{[1]H} and [27]Al{[1]H} CP-MAS experiments were carried out using a 2-ms contact time during which an adiabatic-passage pulse was applied on the ^{1}H channel. The adiabatic cross-polarization was used because it gave a significant increase in the intensity, compared to Hartmann—Hahn cross-polarization.[39]

NMR lineshape analyses were conducted using the software "dmfit #20090330", with Gaussian lineshapes fit according to signal amplitude, position, and width.[40] 1D [29]Si and [27]Al MAS spectra were deconvoluted by collectively fitting peak positions that were subsequently kept the same across spectra obtained for similar samples but acquired using different [29]Si T_1 filter times (Supporting Information, Figures S4—S6).

Solid-state 2D [29]Si{[1]H} and [27]Al{[1]H} HETCOR experiments were conducted to obtain information on molecular interactions between different [29]Si or [27]Al moieties and dipole—dipole-coupled ^{1}H associated with water or hydroxyl groups in the cements. The 2D HETCOR experiment is similar to the 1D CP-MAS technique, with the key exception that the ^{1}H magnetization is allowed to evolve for an incremented evolution time t_1 prior to magnetization transfer to heteronuclei, such as [29]Si or [27]Al, whose responses are measured directly during the detection period t_2.[41] To aid detection of weakly dipole—dipole-coupled spin pairs and/or overcome constraints imposed by rapid spin-relaxation of quadrupolar nuclei (e.g., [27]Al), ^{1}H magnetization can be stored after the evolution period, during which ^{1}H spin-diffusion can occur (along with T_1 relaxation), to distribute magnetization to more distant or mobile moieties before transfer to [29]Si or [27]Al nuclei for detection.[42,43] Double Fourier transformation converts the time-domain signal

(36) Skibsted, J.; Jakobsen, H. J. *J. Chem. Soc., Faraday Trans.* **1995**, *91*, 4423—4430.

(37) Mao, J. D.; Schmidt-Rohr, K. *Solid State Nucl. Magn. Reson.* **2004**, *26*, 36—45.

(38) Gullion, T.; Schaefer, J. *J. Magn. Reson.* **1989**, *81*, 196—200.

(39) Christiansen, S. C.; Hedin, N.; Epping, J. D.; Janicke, M. T.; del Amo, Y.; Demarest, M.; Brzezinski, M.; Chmelka, B. F. *Solid State Nucl. Magn. Reson.* **2006**, *29*, 170—182.

(40) Massiot, D.; Fayon, F.; Capron, M.; King, I.; Le Calve, S.; Alonso, B.; Durand, J. O.; Bujoli, B.; Gan, Z. H.; Hoatson, G. *Magn. Reson. Chem.* **2002**, *40*, 70—76.

(41) Ernst, R. R.; Bodenhausen, G.; Wokaun, A. *Principles of Nuclear Magnetic Resonance in One and Two Dimensions*; Oxford University Press: New York, 1997.

(42) Janicke, M. T.; Landry, C. C.; Christiansen, S. C.; Kumar, D.; Stucky, G. D.; Chmelka, B. F. *J. Am. Chem. Soc.* **1998**, *120*, 6940—6951.

(43) Schmidt-Rohr, K.; Clauss, J.; Spiess, H. W. *Macromolecules* **1992**, *25*, 3273—3277.

$S(t_1, t_2)$ into the frequency domain $F(\omega_1, \omega_2)$, which is typically presented as a 2D contour plot spectrum.[41] The 2D $^{29}Si\{^1H\}$ and $^{27}Al\{^1H\}$ spectra were acquired with frequency-switched Lee−Goldberg (FSLG) homonuclear decoupling during the ^1H evolution period and a ^1H radio frequency field strength of 70 kHz was used to enhance resolution in the ^1H dimension. The 2D experiments (for both ^{29}Si and ^{27}Al) were acquired with 64 t_1 increments of 24 μs each, 3024 transients, and using a recycle delay of 0.7 s that resulted in an experimental time of 27 h for each 2D experiment. The ^1H and ^{29}Si chemical shifts were referenced to tetramethylsilane (TMS) using TKS as a secondary standard, and the ^{27}Al chemical shifts were referenced to an aqueous solution of 0.5 M aluminum nitrate [$Al(NO_3)_3$].

High-resolution solid-state single-pulse ^{27}Al experiments were carried out on a Bruker AVANCE III NMR spectrometer with an 18.8 T standard-bore superconducting magnet and operating at frequencies of 800.43 MHz for ^1H and 208.56 MHz for ^{27}Al. The measurements were performed at room temperature under 20 kHz MAS conditions using a Bruker 3.2 mm H-X-Y triple-resonance probehead with zirconia rotors and Kel-F caps. The high magnetic field mitigates the effects of quadrupolar interactions and yields improved signal sensitivity and resolution of the ^{27}Al species in both the anhydrous and hydrated cements. The quantitative single-pulse ^{27}Al NMR measurements were calibrated using a dense 4.7 mg piece of AlN as an external reference for ^{27}Al spin counting (as opposed to an internal AlN reference, where the ^{27}Al signal overlapped with ^{27}Al species in the cements). To ensure quantitativeness, the AlN spin-counting standard was separately measured using a $\pi/12$ or a $\pi/6$ pulse[44] and a 60 s recycle delay under otherwise identical conditions, which yielded identical results. The single-pulse ^{27}Al spectra were consequently acquired using a high-power 1-μs $\pi/6$ excitation pulse with a recycle delay of 60 s for the AlN sample or 1 s for the cement samples to allow for full relaxation of the ^{27}Al species.

Results and Discussion

The macroscopic properties of hydrated Portland and oilwell cements depend strongly on the molecular-level compositions and structures of the anhydrous starting materials and their reactions with water to form hydrated solid products. The strength of the cement develops as the hydration reactions that promote cross-linking of the silicate species progress. These include reactions of water with dicalcium silicate (C_2S), tricalcium silicate (C_3S), tricalcium aluminate (C_3A), and aluminoferrite (C_4AF) to form ettringite, CSH, and other hydration products, along with adsorption of water on particle surfaces. 1D and 2D solid-state NMR techniques yield a powerful combination of complementary measurements and analyses that shed insights on molecular environments in cement systems, both before and as a result of hydration, from which relative component concentrations, bulk and surface structures, and their interactions with water species can be determined.

Silicate Species in White Portland Cement

The chemical changes that silicate species undergo during hydration are crucial to the setting behavior and strength development of hydrated cements. For example, Ca_3SiO_5 (C_3S) and Ca_2SiO_4 (C_2S) react with water to form CSH and portlandite, $Ca(OH)_2$, that eventually solidify. CSH and other hydration products can be examined by using solid-state ^{29}Si NMR to monitor silicate species with different extents of condensation and hydration.
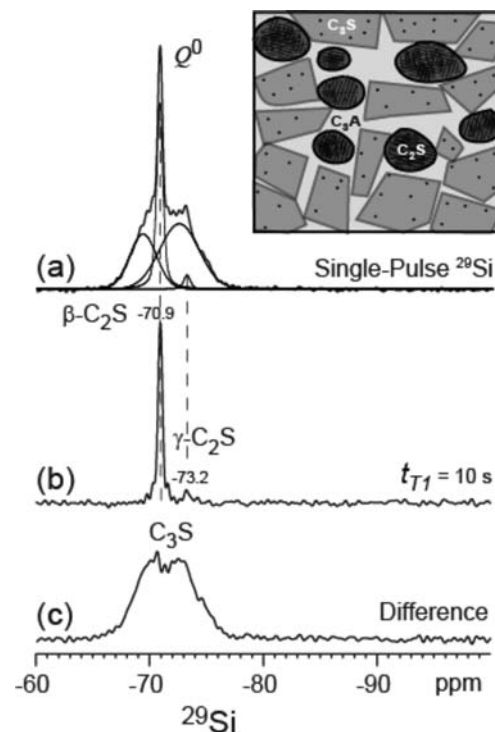
(44) Massiot, D.; Bessada, C.; Coutures, J. P.; Taulelle, F. *J. Magn. Reson.* **1990**, *90*, 231–242.

Figure 1. Solid-state 1D ^{29}Si MAS NMR spectra of anhydrous white Portland cement acquired at room temperature under MAS conditions of 5 kHz with a 60 s recycle delay and different nuclear spin−lattice relaxation-time filter delays (t_{T1}) before detection: (a) a single-pulse ^{29}Si MAS spectrum ($t_{T1} = 0$ s), which yields ^{29}Si signals from all of the silicate species within the di- and tricalcium silicate (C_2S and C_3S) phases; (b) a long t_{T1} of 10 s, which selectively suppresses signals from the C_3S ^{29}Si species, yielding ^{29}Si signals from predominantly C_2S phases; and (c) the difference spectrum between (a) and (b), with (b) scaled by a factor $c = 1.3$. Peak deconvolutions are shown in (a), based on the signals resolved in (b) and (c). The inset shows a schematic diagram of grain structures in the anhydrous white Portland cement, with C_3S represented by the gray polygons, C_2S represented by dark ellipses, and Fe^{3+} ions within the C_2S and C_3S domains represented by black dots. The interstitial matrix is principally composed of the C_3A phase.

Anhydrous White Portland Cement: ^{29}Si NMR. The resolution of ^{29}Si signals from species with low or complicated degrees of molecular order is generally challenging and often limits the information available even from anhydrous cements. For example, a solid-state 1D single-pulse ^{29}Si MAS NMR spectrum of anhydrous white Portland cement in Figure 1a shows overlapping ^{29}Si signals associated with the C_2S and C_3S phases that make the identification of specific chemical moieties and their quantification difficult. The schematic diagram in Figure 1a indicates the principal components of which anhydrous white Portland cement is composed, though about which much remains unknown at a molecular level, particularly with respect to their local structures.

Improved spectral resolution of silicate species with distinct molecular compositions and structures can be achieved by exploiting differences in their local environments to reduce the overlap of their ^{29}Si NMR signals. For example, solid-state NMR techniques can use differences in longitudinal nuclear spin−lattice relaxation times (T_1) to resolve overlapping ^{29}Si signals from different species. T_1 relaxation times are sensitive to molecular motions and structures, including proximities to dipole−dipole-coupled, quadrupolar, or para/ferromagnetic species or chemical shift anisotropies that depend on local bonding configurations. Different silicate components in cements can be distinguished by their different ^{29}Si T_1 relaxation times,[28] which are influenced

significantly by their proximities to para/ferromagnetic species, such as Fe^{3+}. Furthermore, such proximities change during cement hydration processes.[6] The resolution of ^{29}Si signals from different silicate components in solid-state ^{29}Si NMR spectra can be improved by applying a T_1 filter prior to ^{29}Si NMR signal detection. This is achieved by inserting a time delay t_{T1}, during which fast-relaxing ^{29}Si signals ($T_1 < t_{T1}$, such as from species near iron components) decay away, while slow-relaxing ^{29}Si signals ($T_1 > t_{T1}$) persist. This is demonstrated in the 1D ^{29}Si MAS spectrum in Figure 1b, where the application of a relatively long ^{29}Si T_1 filter ($t_{T1} = 10$ s) results in essentially complete suppression of the broad signal between ca. -67 and -76 ppm, while narrow ^{29}Si signals at -70.9 and -73.2 ppm remain. A difference spectrum in Figure 1c (corresponding to the spectrum in Figure 1b subtracted from that in Figure 1a, such that the ^{29}Si peaks at -70.9 and -73.2 ppm are subtracted out), yields the broad ^{29}Si NMR signal intensity between -67 and -76 ppm. The narrow slow-relaxing ^{29}Si signals that are clearly resolved at -70.9 and -73.2 ppm in Figure 1b are assigned to the β and γ polymorphs, respectively, of dicalcium silicate (C_2S), while the broad fast-relaxing ^{29}Si NMR signals in Figure 1c are assigned to the multiple polymorphs of C_3S.[36] Note that although the C_3S polymorphs are crystalline, as manifested by their narrow X-ray diffraction reflections (Supporting Information, Figure S1a), they yield broad ^{29}Si NMR signals, principally due to broadening from para/ferromagnetic iron impurities that also account for their short T_1 relaxation properties. A beneficial consequence of this is that the ^{29}Si NMR signals from silicate moieties in the γ-C_2S, β-C_2S, and C_3S phases are separated, and as a result, their relative populations can be subsequently quantified.

The relative concentrations of the different di- and tricalcium silicate ^{29}Si species are determined by integrating and comparing the relative areas of their signals in 1D single-pulse ^{29}Si MAS NMR spectra. Although poorly resolved in Figure 1a, the different signals in the single-pulse ^{29}Si MAS spectrum of anhydrous Portland cement can be confidently deconvoluted by using the positions, widths, and relative intensities of the respective peaks established in the well-resolved T_1-filtered ^{29}Si spectra of Figure 1b,c. For example, the relative amounts of γ-C_2S, β-C_2S, and C_3S silicate phases are determined by cofitting the overlapping ^{29}Si signals from their respective moieties in Figure 1a, with the well resolved β- and γ-C_2S ^{29}Si signals in Figure 1b and those of the broad ^{29}Si C_3S intensity in Figure 1c. Subsequent integration of the deconvoluted ^{29}Si MAS signals allows the relative fractions of ^{29}Si atoms to be apportioned among the different γ-C_2S, β-C_2S, and C_3S phases in anhydrous white Portland cement and to be quantitatively established as 2 ($\pm$1)%, 26 ($\pm$2)%, and 72 ($\pm$6)%, respectively. Thus, on the basis of the quantitative ^{29}Si lineshape analyses, the ratio of C_3S to C_2S phases is established to be 2.6 ($\pm$0.4). This is in close agreement with a C_3S/C_2S ratio of 2.4 ($\pm$0.1) estimated independently from Rietveld analysis of the XRD pattern of anhydrous white Portland cement (Supporting Information, Figure S1a, Table S2).

Insights into the molecular compositions of anhydrous C_3S and C_2S phases in white Portland cement are gained from analyses of the spin–lattice (T_1) relaxation times of the different ^{29}Si nuclei in these phases. As discussed above, spin–lattice relaxation times in cement are strongly influenced by nearby para/ferromagnetic species, such as Fe^{3+}. The presence of iron in the white Portland cement was separately confirmed by X-ray fluorescence, with an estimated concentration of 0.35 wt % of

Fe_2O_3 (Table 1). Despite the relatively low concentration of iron in the white Portland cement, the strong para- or ferromagnetic effects of these iron components are expected to be sufficient to reduce substantially the ^{29}Si T_1 relaxation times of nearby silicate species within the C_2S and C_3S phases, which are crystalline (Supporting Information, Figure S1a). In crystalline silicates, ^{29}Si T_1 relaxation times can be on the order of thousands of seconds,[29] whereas ^{29}Si T_1 values for silicate species in the C_2S and C_3S phases in white Portland cements are less than 60 s.[36] The shorter ^{29}Si T_1 value (<10 s) measured for the ^{29}Si species in the C_3S phase is attributed to a higher concentration of Fe^{3+} species, compared to the ^{29}Si species in the C_2S phase for which a longer ^{29}Si T_1 time ($\sim$20 s) is observed. The C_3S phases in Portland cement have generally been reported to have higher concentrations of Fe^{3+} ions than C_2S,[45] which is consistent with their different ^{29}Si T_1 properties and broader ^{29}Si signal intensity that are expected also to be influenced by the distributions of Fe species within the different phases.

Hydrated White Portland Cement: ^{29}Si NMR. Hydrated Portland cement is substantially more complicated than the anhydrous starting material because the mixture of different species includes many with distributions of local environments without long-range order, exacerbating resolution challenges from overlapping ^{29}Si signals. Nevertheless, similar single-pulse and T_1-filtered ^{29}Si NMR measurements allow molecular changes that occur to silicate species within the C_2S and C_3S phases during hydration to be quantitatively assessed. (The average bulk compressive strength of the hydrated white Portland cement used here was measured to be ca. 40 MPa, following hydration at room temperature for 28 days.) Compared to the results in Figure 1 above, the 1D single-pulse ^{29}Si MAS NMR spectrum in Figure 2a of hydrated white Portland cement exhibits reduced ^{29}Si signal intensity over the range -67 to -76 ppm, which indicates that the silicate species within the C_3S phase have reacted to form hydration products. In contrast, there appear to be few, if any, changes in the intensities of the ^{29}Si signals at -70.9 and -73.2 ppm from silicate species within the β-C_2S and γ-C_2S phases, respectively, indicating that these phases are largely unaffected by hydration under the conditions used. Additionally, unlike for the anhydrous cement, broad upfield ^{29}Si signals are observed at ca. -79, -82, and -84 ppm, which are overlapping and attributed to Q^1, $Q^2(1Al)$, and Q^2 silicate species, respectively. These arise from the poorly ordered and partially cross-linked CSH component produced by hydration of the C_3S phase. The stoichiometry of CSH (e.g., Ca/Si ratio) depends on the concentration of calcium hydroxide in the aqueous solution, which affects the resulting structure of the CSH product.[2] The relatively high Ca:Si ratios (ca. 1.7) characteristic of CSH associated with Portland cements are thought to contribute to the formation of short disordered chains of condensed silicate tetrahedra.[6] This is consistent with the broad and overlapping ^{29}Si signals from the different partially condensed Q^1 and Q^2 silicate species in Figure 2a.

As for the anhydrous cement, the application of a ^{29}Si T_1 filter to the hydrated white Portland cement reduces overlap of the ^{29}Si signals that arise from the complicated mixture of hydrated and anhydrous cement components. By using such a ^{29}Si T_1 filter (10 s), the different ^{29}Si species in the C_3S, C_2S, and CSH components can be distinguished and their transforma-

(45) Poulsen, S. L.; Kocaba, V.; Le Saout, G.; Jakobsen, H. J.; Scrivener, K. L.; Skibsted, J. *Solid State Nucl. Magn. Reson.* **2009**, *36*, 32–44.
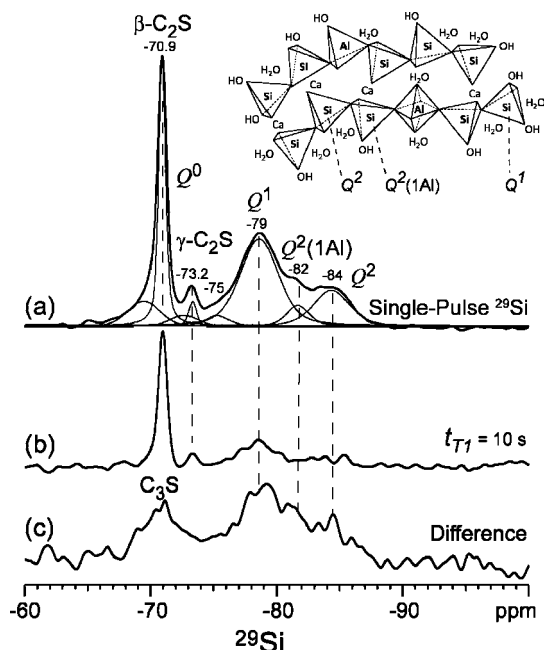
Figure 2. Solid-state 1D ^{29}Si MAS NMR spectra of hydrated white Portland cement acquired at room temperature, 5 kHz MAS, with a 60 s recycle delay and different spin–lattice relaxation-time filters (t_{T1}) before detection: (a) a single-pulse ^{29}Si MAS spectrum ($t_{T1} = 0$ s), which yields ^{29}Si signals from unreacted anhydrous C_2S and C_3S ^{29}Si species, as well as Q^1 and Q^2 species of calcium-silicate-hydrate (CSH); (b) a long t_{T1} of 10 s suppresses ^{29}Si signals from C_3S and a majority of the CSH species, yielding signals predominantly from the C_2S species; and (c) the difference spectrum between (a) and (b), which spectrally resolves ^{29}Si signals from species in C_3S and CSH. Peak deconvolutions are shown in (a), based on the signals resolved in (b) and (c). The inset shows a schematic diagram of the CSH component and different four-coordinate Q^1 and Q^2 silicate and six-coordinate Al molecular moieties.

tions and proximities to iron-containing moieties in the hydrated white Portland cement established. As shown in Figure 2b, the ^{29}Si-T_1 filtered spectrum exhibits signals at −70.9 and −73.2 ppm from the ^{29}Si species in C_2S at the same relative intensities as in Figure 1b, consistent with the retention of the C_2S phase in the hydrated cement. The broad signal(s) in the range −67 to −76 ppm from the ^{29}Si species in C_3S are completely absent. Unlike the anhydrous starting material, however, there is additional broad and weak ^{29}Si intensity between −78 and −87 ppm, which is associated with Q^1 and Q^2 silicate species in the CSH. The presence of these upfield signals in the T_1-filtered spectrum indicates that the hydrated products tend to have longer ^{29}Si-T_1 relaxation times than ^{29}Si species in C_3S from which they originate. This might be considered surprising because amorphous hydrated silicates like CSH typically exhibit shorter ^{29}Si-T_1 relaxation times compared to crystalline phases, such as C_3S. However, it is the relatively high Fe^{3+} content in crystalline C_3S that accounts for its rapid ^{29}Si spin-relaxation behavior, compared to the amorphous CSH product, which apparently incorporates less Fe^{3+}.

It is hypothesized that during the hydration reaction of C_3S to form CSH, the Fe species located within the C_3S phase are not fully incorporated into the CSH hydration product(s) and that the hydrated Fe species segregate into a separate component(s). Para- or ferromagnetic Fe species and their distributions are challenging to characterize because they are often in disordered environments in cementious materials and complicated by the multicomponent nature of the mixtures. The scaled difference spectrum shown in Figure 2c (Figure 2b subtracted

from Figure 2a) exhibits no ^{29}Si signals from the C_2S phases and reduced overlap between the ^{29}Si signals of C_3S and CSH, consistent with Fe partitioning away from the CSH product species. Thus, solid-state single-pulse and T_1-filtered ^{29}Si NMR measurements show that, during hydration of white Portland cement, C_3S reacts to form disordered CSH, which is composed of Q^1, Q^2(1Al), and Q^2 silicate moieties that are less closely associated with Fe than in the initial anhydrous C_3S. Previous studies have reported segregation of Fe species during hydration of aluminoferrite (C_4AF),[46−48] which is not present to a significant extent in white Portland cement (Tables 1 and S2, Supporting Information); less is known about Fe partitioning among the different silicate components. Additional work is currently underway in our laboratories to characterize these iron species and their distributions in hydrated cements.

To examine in greater molecular detail the CSH component directly, it is necessary to apply a ^{29}Si NMR filter that distinguishes the local environments of different partially cross-linked silicate species. Though the isotropic ^{29}Si chemical shifts of these moieties overlap and their ^{29}Si T_1 relaxation times are similar, they possess different ^{29}Si chemical shift anisotropies that reflect the distinct local ^{29}Si bonding symmetries of the different hydrated silicate species. Larger ^{29}Si chemical shift anisotropies are associated with less symmetrical bonding environments. Consequently, a CSA filter can be used to resolve and quantify different ^{29}Si sites in CSH to provide new insights into their molecular compositions and structures.

The CSA filter is based on recoupling ^{29}Si CSA interactions, which are sensitive to the different bonding environments of Q^1 and Q^2 ^{29}Si sites in CSH. Although ^{29}Si CSA interactions are averaged by fast MAS, they can be reintroduced by recoupling techniques[37] that allow the ^{29}Si NMR signals of silicate species with the greater CSAs to be selectively suppressed (dephased). Figure 3 shows solid-state ^{29}Si MAS spectra of hydrated white Portland cement that were acquired under identical conditions, except for variation of the time (t_{csa}) over which the CSA filters were applied. Using a short 1-μs CSA recoupling time yields a ^{29}Si MAS spectrum (Figure 3a) that is identical to the single-pulse spectrum in Figure 2a, indicating that no dephasing of the ^{29}Si silicate species has occurred. For a substantially longer recoupling time of 43 μs, the resulting spectrum in Figure 3b exhibits ^{29}Si signals principally at −70.9, −73.2, and −79 ppm from the Q^0 (C_2S) and Q^1 species, respectively, which have relatively small CSAs that are not appreciably dephased. By comparison, the Q^2 and Q^2(1Al) ^{29}Si signals at −82 and −84 ppm are suppressed, consistent with the larger CSAs associated with their less symmetric local ^{29}Si bonding environments.[49] The difference spectrum in Figure 3c shows enhanced ^{29}Si intensity from the Q^2 and Q^2(1Al) moieties, together with signals from Q^0 and Q^1 species that were partially suppressed in Figure 3b. The CSA filter thus provides improved resolution of Q^1 ^{29}Si resonances from otherwise overlapping Q^2 and Q^2(1Al) ^{29}Si signals in the CSH.

Quantification of ^{29}Si Species in White Portland Cement. The combined application of T_1 and CSA filters permits the ^{29}Si

(46) Brown, P. W. *J. Am. Ceram. Soc.* **1987**, *70*, 493–496.
(47) Bishop, M.; Bott, S. G.; Barron, A. R. *Chem. Mater.* **2003**, *15*, 3074–3088.
(48) Millogo, Y.; Hajjaji, M.; Ouedraogo, R.; Gomina, M. *Constr. Build. Mater.* **2008**, *22*, 2078–2086.
(49) The Q^0 ^{29}Si species have close to tetrahedral (C_4) symmetry and thus the smallest CSAs, while the Q^1 ^{29}Si species have closer to C_3 symmetry and Q^2 ^{29}Si species approximately C_2 symmetry, with correspondingly larger CSAs, respectively.
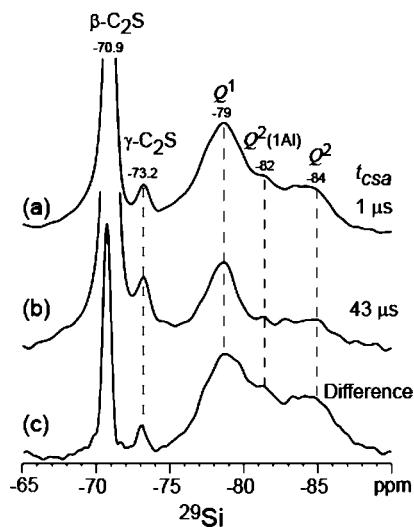
Figure 3. Solid-state 1D ^{29}Si MAS NMR spectra of hydrated white Portland cement (same as in Figure 2) acquired at 278 K and 5 kHz MAS, with 10 s recycle delay, and different chemical-shift-anisotropy (CSA) filter times (t_{csa}) before detection: (a) $t_{csa} = 1$ μs, which yields ^{29}Si signals from the different ^{29}Si species and (b) $t_{csa} = 43$ μs, which preferentially suppresses ^{29}Si signals from Q^2 and Q^2 (1Al) species, thereby improving the resolution of Q^1 ^{29}Si signals. (c) A scaled difference spectrum between the (a) and (b) shows enhanced signal intensity associated with the Q^2 and Q^2 (1Al) sites, whose lower local ^{29}Si bonding symmetries are characterized by larger CSA values.

Table 2. Relative Site Populations of NMR-Visible ^{29}Si Species in the Anhydrous and Hydrated White Portland Cements Used in This Study

anhydrous white Portland cement			hydrated white Portland cement		
assignment	^{29}Si signal (ppm)	relative % of visible ^{29}Si	assignment	^{29}Si signal (ppm)	relative % of visible ^{29}Si
Q^0, C$_3$S	−69	26 (±3)	Q^0, C$_3$S	−69	8 (±2)
Q^0, β-C$_2$S	−70.9	26 (±2)	Q^0, β-C$_2$S	−70.9	26 (±1)
Q^0, C$_3$S	−73	46 (±3)	Q^0, C$_3$S	−73	3 (±2)
Q^0, γ-C$_2$S	−73.2	2 (±1)	Q^0, γ-C$_2$S	−73.2	2 (±1)
			Q^0	−75	3 (±2)
			Q^1	−79	38 (±3)
			Q^2(1Al)	−82[a]	6 (±3)
			Q^2	−84[a]	14 (±3)

[a] Overlap of ^{29}Si signals associated with Q^2 and Q^2 (1Al) species in both T_1- and CSA-filtered spectra persists, resulting in additional uncertainty in the relative populations of these two species.

signals and lineshapes of key silicate species in the hydrated white Portland cement to be distinguished and enables their relative populations to be quantified. The relative concentrations of different silicate species are determined by integrating Gaussian lineshape fits to the overlapping signals in the quantitative single-pulse ^{29}Si MAS spectrum of Figure 2a. These fits are based on the T_1- and CSA-resolved lineshapes in Figure 2b,c and Figure 3b, respectively, which increase the confidence of the analyses that yield the relative concentrations of the different silicate species tabulated in Table 2. It is noteworthy that the Q^0 signals at −70.9 and −73.2 ppm associated with the dicalcium silicate phases are measured to be 26% and 2% for the β- and γ-C$_2$S, respectively, the same as for the anhydrous cement. This indicates that these phases are not significantly affected by hydration for the conditions used and within the experimental uncertainties of the NMR measurements. By comparison, the Q^0 species associated with the tricalcium silicate phases (−69 and −73 ppm) are measured to be 8% and 3% in the hydrated cement, compared to 26% and 46% in the
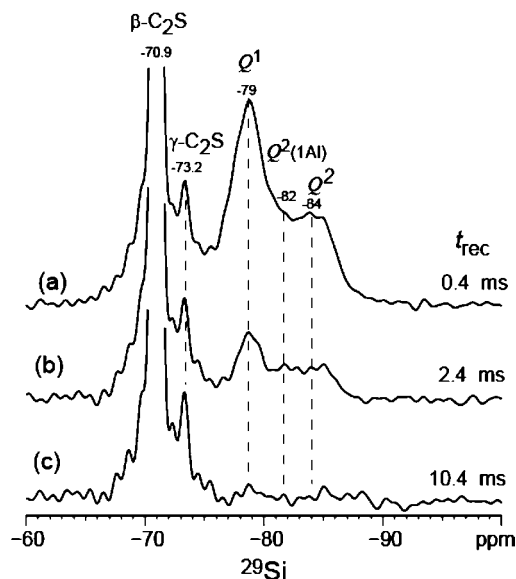

Figure 4. Solid-state 1D ^{29}Si{^{1}H} rotational-echo double-resonance (RE-DOR) spectra of hydrated white Portland cement (same as in Figures 2 and 3) acquired at 278 K and 5 kHz MAS, using a 10 s recycle delay with different dipolar ^{1}H−^{29}Si dipolar recoupling times (t_{rec}): (a) $t_{rec} = 0.4$ ms, (b) $t_{rec} = 2.4$ ms, and (c) $t_{rec} = 10.4$ ms.

anhydrous starting material, consistent with their preferential consumption during hydration.[6] Integration of the lineshape fits to ^{29}Si signals at −79, −82, and −84 ppm, establish the approximate mole percentages of the cross-linked Q^1, Q^2(1Al), and Q^2 ^{29}Si moieties to be 38%, 6%, and 14%, respectively, in the CSH. These results are consistent with the formation of cross-linked silicate species in hydrated white Portland cement and are suggestive of interactions among the silicate and aluminate moieties during setting.

Hydrated Silicate Species in White Portland Cement. Interactions between different silicate and hydrogen-containing species within hydrated cements can be probed by using ^{29}Si REDOR NMR, which is sensitive to the strengths of ^{1}H−^{29}Si dipolar interactions. Silicate moieties in CSH, in particular, are expected to contain hydroxyl groups and/or interact with adsorbed water, although specific interactions have not been established. By reintroducing the ^{1}H−^{29}Si dipolar interactions under MAS conditions using the REDOR technique,[38] the ^{29}Si signals of silicate species interacting with protons are dephased, according to the strengths of their heteronuclear dipole−dipole couplings. Figure 4 shows the 1D ^{29}Si{^{1}H} REDOR spectra of hydrated white Portland cement acquired using different dipolar recoupling times (t_{rec}), the longer durations of which engage progressively weaker ^{29}Si−^{1}H dipolar interactions. For a short recoupling time (0.4 ms, Figure 4a), a ^{29}Si{^{1}H} REDOR spectrum is obtained that is similar to the single-pulse ^{29}Si MAS spectrum (Figure 2a), indicating negligible dephasing of the resolved ^{29}Si species present. By comparison, the use of a longer recoupling time (2.4 ms, Figure 4b) yields a REDOR spectrum with pronounced intensity over the range −67 to −76 ppm from the anhydrous Q^0 C$_2$S and C$_3$S ^{29}Si moieties but significantly suppressed intensity from the Q^1 and Q^2 signals (−78 to −88 ppm) associated with CSH that are dephased. Use of a longer recoupling time (10.4 ms, Figure 4c) results in a REDOR spectrum in which the Q^1, Q^2, and Q^2(1Al) ^{29}Si signals are completely dephased and absent. These results establish that the Q^1, Q^2, and Q^2(1Al) moieties of the CSH product are in close proximities (ca. 1 nm) to hydrogen-containing species.
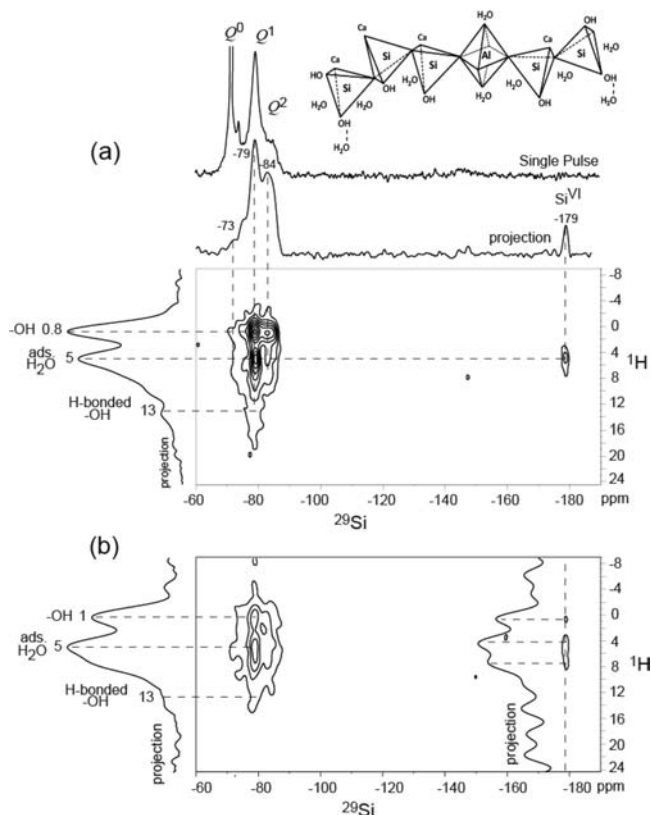
Figure 5. Solid-state 2D ^{29}Si{^{1}H} HETCOR spectra of hydrated white Portland cement (same as in Figures 2−4) acquired at 278 K and 6.5 kHz MAS, with 0.5 s recycle delay and different ^{1}H spin-diffusion times t_{sd} of (a) $t_{sd} = 10$ μs and (b) $t_{sd} = 30$ ms. Along the top horizontal axis, a 1D single-pulse ^{29}Si MAS spectrum is shown for comparison above the 1D ^{29}Si projection of the 2D spectrum. 1D projections of the ^{1}H dimension of the 2D spectra are shown along the vertical axes on the left. The lowest contour lines shown in the 2D spectra are 15% of maximum intensity. Inset: schematic diagram of the calcium-silicate-hydrate (CSH) component illustrating its interactions with hydroxyl groups and adsorbed or hydrogen-bonded water.

Furthermore, the ^{29}Si signal from the dimeric Q^1 species (which are at the ends of cross-linked silicate chains) dephase more rapidly than those associated with the Q^2, and Q^2(1Al) moieties, indicating that the Q^1 species interact more strongly with nearby protons, although the specific species cannot be determined on the basis of the REDOR results alone.

The specific molecular interactions between various ^{29}Si and ^{1}H species in the CSH can be determined by using 2D NMR methods to characterize the local composition and structure of hydrated white Portland cement in detail. 2D ^{29}Si{^{1}H} HETCOR spectra provide dramatically increased resolution of ^{29}Si and ^{1}H signals by spreading them into a 2D frequency map. Such a map permits otherwise overlapping signals to be separated and allows correlations between specific molecular moieties to be established.[50] For example, Figure 5 shows 2D ^{29}Si{^{1}H} HETCOR contour-plot spectra of the same hydrated white Portland cement studied in Figures 2−4, with a separately acquired 1D single-pulse ^{29}Si MAS spectrum plotted along the top horizontal axis to aid the interpretation of the 2D data. Both

of the 2D spectra were acquired under identical conditions, except for variation of the ^{1}H spin-diffusion time (10 μs versus 30 ms) that allow for weaker ^{29}Si−^{1}H dipole−dipole-coupled spin-pairs to be probed at longer times. The dotted lines indicate intensity correlations observed, and the 1D projections of the signals along the respective axes permit specific species to be identified and compared with the single-pulse ^{29}Si MAS spectrum.

For a short spin-diffusion time, correlated signal intensity in the 2D spectrum is observed only for strongly coupled species that have sufficiently high populations, are molecularly near (<1 nm), and have relatively low molecular mobilities. A 2D ^{29}Si{^{1}H} HETCOR spectrum of hydrated white Portland cement acquired using a very short spin-diffusion time (10 μs) is shown in Figure 5a. The horizontal dotted lines and 1D projection in the ^{1}H dimension (left) reveal signals from at least three types of ^{1}H species corresponding to −OH groups (0.8 ppm), adsorbed H$_2$O (5 ppm), and strongly hydrogen-bonded −OH species (∼13 ppm). These assignments are based on previous ^{1}H NMR studies of crystalline silicates and aluminosilicates,[29,51,52] silicas or aluminosilicas,[42,53] and CSH[33] that show proton species associated with terminal SiOH, CaOH, and AlOH resonate between −1 and +3 ppm, adsorbed H$_2$O between 3 and 6 ppm, and hydrogen-bonded SiOH between 6−15 ppm. The vertical dotted lines and 1D projection in the ^{29}Si dimension of the 2D spectrum (Figure 5a) reveal at least four distinct ^{29}Si moieties that strongly interact with the various proton species. A comparison with the accompanying single-pulse ^{29}Si MAS spectrum (top) shows no significant correlated ^{29}Si−^{1}H signal intensity associated with the Q^0 ^{29}Si sites, as expected for unreacted and unhydrated C$_2$S or C$_3$S phases. There are a number of strong and distinct intensity correlations that are resolved between the Q^1, Q^2, and Q^2(1Al) ^{29}Si moieties associated with the CSH and different H$_2$O and −OH species. Specifically, strong intensity correlations are present at 0.8 ppm in the ^{1}H dimension and at −79 ppm and −84 ppm in the ^{29}Si dimension, which can therefore be assigned to silanol groups associated with partially cross-linked Q^1, Q^2, and Q^2(1Al) moieties of the CSH. Although the majority of the −OH species are expected to be directly bonded to ^{29}Si species, some may also be associated with CaOH moieties that are incorporated within the CSH product. A strong intensity correlation is also observed at a ^{1}H shift of 5 ppm and a ^{29}Si shift of −79 ppm, which establishes strong interactions of the Q^1 species and adsorbed water. Such combined interactions with both hydroxyl species and adsorbed water accounts for the relatively fast dephasing of the Q^1 ^{29}Si signals, as previously observed and discussed for the REDOR spectra (Figure 4). The inset in Figure 5a depicts a schematic structure of CSH that is consistent with these 1D and 2D ^{29}Si NMR results.

Weaker intensity correlations in the 2D ^{29}Si{^{1}H} HETCOR spectrum of Figure 5a reflect weaker interactions or lower concentrations of dipole−dipole-coupled species. For example, weak correlated signal intensity is observed in the range 0−5 ppm in the ^{1}H dimension and at a ^{29}Si shift of −73 ppm, which indicates interactions between adsorbed water or hydroxyl groups and Q^0 ^{29}Si species in C$_3$S that may be near particle surfaces, though not yet cross-linked to form Q^1 species. Weak 2D intensity is also observed over the range 10−18 ppm in the

(50) Dipole−dipole interactions occur between NMR-active ^{1}H and ^{29}Si nuclei, so that the 2D ^{29}Si{^{1}H} HETCOR measurements apply strictly to these nuclei. The chemical interactions and conclusions based on the 2D ^{29}Si{^{1}H} HETCOR spectra are applicable to the more abundant ^{28}Si atoms in cements as well.

(51) Fleischer, U.; Kutzelnigg, W.; Bleiber, A.; Sauer, J. *J. Am. Chem. Soc.* **1993**, *115*, 7833−7838.

(52) Hunger, M. *Solid State Nucl. Magn. Reson.* **1996**, *6*, 1−29.

(53) Hunger, M.; Freude, D.; Pfeifer, H. *J. Chem. Soc., Faraday Trans.* **1991**, *87*, 657−662.

^{1}H dimension and at −79 ppm in the ^{29}Si dimension, corresponding to hydrogen-bonded −OH groups at Q^1 silicate sites. Interestingly, though not visible in the single-pulse ^{29}Si MAS spectrum, correlated signal intensity is clearly observed at a ^{1}H shift of 5 ppm and a low-frequency ^{29}Si shift of −179 ppm, indicating strongly adsorbed water at six-coordinate silicate sites, the latter of which have been previously observed in calcium silicate minerals formed under extreme conditions of temperature and pressure (e.g., deep within the earth's mantle or during meteorite impacts).[54] The ^{29}Si^{VI} species observed here are associated with the mineral thaumasite, a unique silicate formed in Portland cement under ambient conditions with the chemical formula $[Ca_3Si(OH)_6 \cdot 12H_2O](SO_4)(CO_3)$.[55,56] Thaumasite is a highly hydrated phase, with a similar structure to ettringite that is hypothesized to form by the reaction of SO_4^{2-} and CO_3^{2-} with CSH and tends to weaken the cement.[57] The relative narrowness of this signal in both the ^{1}H and ^{29}Si dimensions indicates a narrow distribution of species, which are not sufficiently prevalent to yield a ^{29}Si signal in the single-pulse spectrum, but which can be detected because of the CP-signal enhancement provided by the ^{29}Si{^{1}H} HETCOR experiment. The relative intensities of the correlated signals in the 2D spectra thus provide detailed insights into the local compositions, structures, and interactions of the different molecular components of hydrated white Portland cement.

While ^{29}Si{^{1}H} HETCOR measurements as conventionally applied are sensitive to molecular proximities of ca. 1 nm, the incorporation of longer ^{1}H spin-diffusion times can probe weaker interactions between different ^{1}H and ^{29}Si species over several nanometers.[58] Figure 5b shows a 2D ^{29}Si{^{1}H} HETCOR spectrum of the same hydrated white Portland cement as examined in Figure 5a but acquired with a ^{1}H spin-diffusion time of 30 ms. This much longer effective contact time leads to the appearance of similar correlated ^{29}Si and ^{1}H signals, but with different intensities and broader distributions, as ^{1}H spin-diffusion disperses magnetization to more weakly coupled ^{29}Si moieties and relaxation processes reduce overall signal strength. In particular, correlated intensity is observed between the ^{29}Si signal at −179 ppm from six-coordinate silicate species and ^{1}H resonances at ca. 5 ppm from adsorbed H_2O and a new weak signal at 1 ppm from −OH species. On the basis of these results, a postulated structure of the CSH, including adsorbed water, is shown in inset of Figure 5 (top), which is consistent with the detailed NMR measurements above, recent molecular modeling analyses,[59] small-angle neutron and X-ray scattering data,[60] and transmission electron microscopy studies.[61] The 2D ^{29}Si{^{1}H} HETCOR spectra reveal numerous new molecular insights on the complicated composition and structure of hydrated white
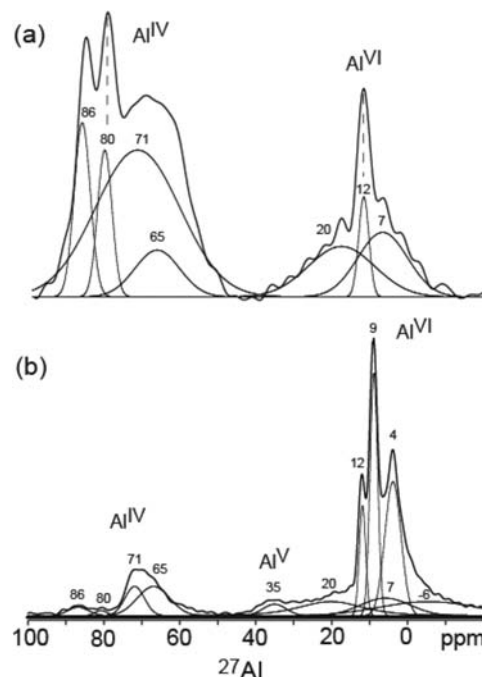

Figure 6. Solid-state 1D single-pulse ^{27}Al MAS NMR spectra acquired at 18.8 T at 278 K and 20 kHz MAS for (a) anhydrous and (b) hydrated white Portland cement. Deconvolution fits to the spectra are shown, along with their respective peak positions.

Portland cement, particularly with respect to different interactions between the silicate and hydroxyl/water species present.

Aluminate Species in White Portland Cement

Anhydrous and Hydrated White Portland Cement: ^{27}Al NMR. The interactions of the different aluminate species present in white Portland cement with water and silicate species influence the setting and strength of the hydrated cement significantly. These interactions and the changes that occur upon hydration can be monitored by solid-state ^{27}Al MAS NMR measurements conducted at very high magnetic fields to resolve ^{27}Al signals in different molecular environments. For example, the single-pulse ^{27}Al MAS spectrum shown in Figure 6a of anhydrous white Portland cement acquired at 18.8 T (800 MHz ^{1}H) and under MAS conditions of 20 kHz yields partially resolved ^{27}Al signals that correspond to different aluminate species. (The Al_2O_3 content of this white Portland cement was determined by X-ray fluorescence to be 2.0 wt %, Table 1.) The two ^{27}Al signals at 80 and 86 ppm correspond to four-coordinate ^{27}Al^{IV} moieties that have previously been attributed to aluminum species within the C_2S and C_3S phases,[4,30,62] with relative distributions of ca. 0.7 wt % and 1.0 wt % of Al_2O_3, respectively.[4,30] The much broader ^{27}Al^{IV} intensity at ca. 70 ppm can be fit to two overlapping signals centered at ca. 71 and 65 ppm that likely arise from a distribution of ^{27}Al^{IV} species in the C_3A phase(s).[63] Within the resolution limits of the spectra, the ^{27}Al MAS signals appear to be inhomogeneously broadened, arising principally from distributions of ^{27}Al sites within the C_2S, C_3S, and C_3A phases of the cements.[64] The ^{27}Al signal at 20 ppm is thought to arise from Al^{VI} species in separate amorphous aluminate grain-boundary components between C_2S

(54) Stebbins, J. F.; Kanzaki, M. *Science* **1991**, *251*, 294–298.
(55) Duffy, J. A.; Macphee, D. E. *J. Phys. Chem. B* **2007**, *111*, 8740–8745.
(56) Skibsted, J.; Rasmussen, S.; Herfort, D.; Jakobsen, H. J. *Cem. Concr. Compos.* **2003**, *25*, 823–829.
(57) Schmidt, T.; Lothenbach, B.; Romer, M.; Scrivener, K.; Rentsch, D.; Figi, R. *Cem. Concr. Res.* **2008**, *38*, 337–349.
(58) Schmidt-Rohr, K.; Spiess, H. W. *Multidimensional Solid-State NMR and Polymers*; Academic Press Limited: London, 1994.
(59) Pellenq, R. J. M.; Kushima, A.; Shahsavari, R.; Van Vliet, K. J.; Buehler, M. J.; Yip, S.; Ulm, F. J. *Proc. Nat. Acad. Sci. U.S.A.* **2009**, *106*, 16102–16107.
(60) Allen, A. J.; Thomas, J. J.; Jennings, H. M. *Nat. Mater.* **2007**, *6*, 311–316.
(61) Xu, Z.; Viehland, D. *Phys. Rev. Lett.* **1996**, *77*, 952–955.

(62) Le Saout, G.; Lecolier, E.; Rivereau, A.; Zanni, H. *Cem. Concr. Res.* **2006**, *36*, 71–78.
(63) Skibsted, J.; Henderson, E.; Jakobsen, H. J. *Inorg. Chem.* **1993**, *32*, 1013–1027.

grains or as inclusions within C_2S grains, which have been observed by electron microscopy[65] and ^{27}Al NMR.[4] The intense narrow [27]Al signal at 12 ppm reflects Al^{VI} species in a symmetric environment that is likely associated with ettringite (a crystalline mineral phase), consistent with XRD reflections of the anhydrous white Portland cement (Supporting Information, Figure S1a) and which is likely formed by adsorption of moisture during storage of the "anhydrous" cement. Additionally, there is a broad [27]Al signal at 7 ppm that may be attributed to six-coordinate Al^{VI} species in the CSH,[62] which are expected to be associated with strongly adsorbed water.

Molecular changes in the aluminate species as a result of hydration can be monitored by single-pulse ^{27}Al MAS NMR of hydrated white Portland cement. As shown in Figure 6b, upon hydration, the $^{27}Al^{IV}$ signals over the range $60-90$ ppm are greatly reduced in intensity, compared to the $^{27}Al^{VI}$ signals between -15 and 15 ppm, which are much more intense and narrower. Single-pulse [29]Si MAS spectra (Figure 2) previously showed that the silicate species in C_3S reacted during hydration and were largely consumed, whereas silicate species in C_2S were mostly unaffected. This suggests that the [27]Al signals at 80 and 86 ppm, which have nearly entirely disappeared in Figure 6b, are most likely associated with silicate species in C_3S rather than C_2S. Similarly, the broad overlapping $^{27}Al^{IV}$ signals between $60-75$ ppm associated with the C_3A species are also significantly less intense after hydration. The disappearance of these [27]Al signals from four-coordinate aluminum moieties is offset by the appearance of significantly more intense $^{27}Al^{VI}$ signals at 12, 9, and 4 ppm that correspond to primary products of aluminate hydration. The dominant $^{27}Al^{VI}$ signal at 9 ppm is assigned to calcium aluminate monosulfate hydrate (AFm),[25] which is an expected reaction product with water. From the narrow peak width (3 ppm, full-width-half-maximum (fwhm)), these $^{27}Al^{VI}$ sites in the AFm phase are locally ordered, consistent with a weak reflection in the XRD pattern (Supporting Information, Figure S1b). The peak at 12 ppm is attributed to $^{27}Al^{VI}$ species in ettringite, as also present in the anhydrous starting material. Recent work[32] suggests that the relatively narrow $^{27}Al^{VI}$ peak at 4 ppm can be assigned to so-called "third-aluminum-hydrate" (TAH) species that may be partially ordered aluminum hydroxide or calcium aluminate hydrate that are not evident by XRD. The narrow line width (5 ppm, fwhm) indicates that the local ^{27}Al environments in the TAH component are relatively uniform, suggesting that they are present in separate domains, perhaps in proximity to the CSH product, but not as Al^{3+} ions substituted for Ca^{2+} ions in the layers of the disordered CSH structure. Broad weak [27]Al signal intensity centered at ca. 35 ppm has been previously attributed to five-coordinate Al^{3+} substituting for Ca^{2+} in the interlayer space of the CSH.[66] A broad weak [27]Al signal at ca. -6 ppm may arise from hydrated products with structures related to $Ca_3Al_2H_{12}O_{12}$ and $Ca_3Al_2Si_3O_{12}$ (termed "hydrogrossular" phases),[6,62] or possibly an aluminate hydrate associated with iron components.

(64) Fitting of the associated [27]Al MAS spectra in Figure 6 to one or more second-order quadrupolar MAS lineshapes does not account for the broadened [27]Al signal intensities observed in the $^{27}Al^{IV}$ region of the spectra. This is consistent with relatively disordered local [27]Al environments that likely arise from distributions of Al sites substituted for Si within these phases.

(65) Chan, C. J.; Kriven, W. M.; Young, J. F. *J. Am. Ceram. Soc.* **1988**, *71*, 713–719.

(66) Faucon, P.; Delagrave, A.; Petit, J. C.; Richet, C.; Marchand, J. M.; Zanni, H. *J. Phys. Chem. B* **1999**, *103*, 7796–7802.

Table 3. Relative Site Populations of NMR-Visible [27]Al Species in the Anhydrous and Hydrated White Portland Cements Used in This Study

anhydrous white Portland cement			hydrated white Portland cement		
assignment	[27]Al signal (ppm)	relative % of visible [27]Al	assignment	[27]Al signal (ppm)	relative % of visible [27]Al
Al^{IV}	86	11 ($\pm$2)	Al^{IV}	86	1 ($\pm$2)
Al^{IV}	80	8 ($\pm$2)	Al^{IV}	80	<1 ($\pm$1)
Al^{IV}	71	45 ($\pm$3)	Al^{IV}	71	6 ($\pm$2)
Al^{IV}	65	9 ($\pm$3)	Al^{IV}	65	9 ($\pm$2)
Al^{V}	35	<1 ($\pm$1)	Al^{V}	35	3 ($\pm$1)
Al^{VI}	20	10 ($\pm$2)	Al^{VI}	20	10 ($\pm$3)
Al^{VI}	12	5 ($\pm$2)	Al^{VI}	12	7 ($\pm$1)
Al^{VI}	9	<1 ($\pm$1)	Al^{VI}	9	19 ($\pm$4)
Al^{VI}	7	12 ($\pm$3)	Al^{VI}	7	10 ($\pm$3)
			Al^{VI}	4	21 ($\pm$4)
			Al^{VI}	-6	14 ($\pm$3)

Quantification of [27]Al Species in White Portland Cement. Compared to ^{27}Al MAS NMR measurements conducted at lower magnetic fields, spectra acquired at 18.8 T exhibit superior resolution of [27]Al signals in cements than has previously been possible. This is due to the diminished contributions from second-order quadrupolar interactions at very high magnetic fields, which can otherwise broaden [27]Al MAS signals. Several of the [27]Al MAS peaks in Figure 6a for anhydrous white Portland cement still overlap and were fit to Gaussian lineshapes and deconvoluted to estimate the relative site populations (Supporting Information, Figure S4a), which are listed in Table 3. This analysis shows that NMR-visible [27]Al species in "anhydrous" white Portland cement are made up of 73% Al^{IV} and 27% Al^{VI} moieties, including approximately 7% ettringite Al^{VI} species. Reduced [27]Al linewidths and increased signal sensitivity at 18.8 T lead to [27]Al MAS spectra with higher resolution than previously achievable, allowing for both improved identification and quantification of the numerous NMR-visible $^{27}Al^{IV}$ and $^{27}Al^{VI}$ species in white Portland cement.

For hydrated white Portland cement, quantitative characterization of Al species by solid-state ^{27}Al NMR under very high magnetic field conditions is expected to provide helpful estimates of [27]Al quantities in both crystalline phases and noncrystalline species. ^{27}Al NMR measurements are complementary to X-ray scattering analyses, the latter of which are generally unsuitable for quantifying the large fraction of noncrystalline components or nonstoichiometric substitutions of Al in otherwise crystalline silicate networks. The solid-state 1D single-pulse [27]Al MAS spectrum shown in Figure 6b acquired at 18.8 T exhibits resolved or partially resolved [27]Al signals that can be assigned to moieties associated with C_2S, C_3S, C_3A, CSH, ettringite, monosulfate, and TAH components. The relatively narrow [27]Al signals from the ettringite, monosulfate, and TAH reaction products, furthermore, indicate that Fe is largely excluded from them. Similar observations have been reported that suggest at least partial partitioning of iron from aluminates in the hydration products of aluminoferrite (C_4AF).[46–48] The [27]Al peaks in the [27]Al MAS spectrum (Figure 6b) of the hydrated white Portland cements were fit to Gaussian lineshapes that allowed the spectra to be deconvoluted to estimate the relative site populations (Supporting Information, Figure S4b), which are listed in Table 3. In particular, the relative concentration of NMR-visible Al^{IV} species decreases from 73% in anhydrous white Portland cement to 16% after hydration, while hydrated Al^{V} and Al^{VI} species associated with ettringite, monosulfate, TAH, and CSH increase from 27% to 84%. These results are consistent with XRD patterns (Supporting

Information, Figure S1) that show reflections from crystalline phases and provide improved molecular-level quantification of both ordered and disordered species in the anhydrous and hydrated white Portland cements.

While ^{27}Al NMR provides detailed insights into the molecular structure of both anhydrous and hydrated white Portland cements, the quadrupolar nature (spin-5/2) of ^{27}Al nuclei, compounded by the line-broadening effects of nearby para/ferromagnetic Fe, means that not all of the ^{27}Al species are equally NMR-visible, making their absolute quantification difficult. To assess the extent of ^{27}Al NMR signal visibility and estimate the absolute populations of the aluminate species whose ^{27}Al signals are observed, a known mass (4.7 mg) of AlN was used as an external calibration standard (see the Experimental Section). This permitted spin-counting the amounts of visible ^{27}Al species in the cements, which were compared to their bulk Al contents separately determined from XRF analyses (Table 1). From such comparisons with quantitative single-pulse spin-counting ^{27}Al NMR measurements, it can be concluded that only 20% of ^{27}Al species are visible by ^{27}Al MAS NMR at 18.8 T in the anhydrous white Portland cement, which increases to 80% after hydration. There is a large precedent in the literature for the presence of "NMR-invisible" ^{27}Al species, which are thought to occupy distorted sites at crystallite surfaces, near defects, or in disordered regions, or especially important for the cement samples here, near ferric ion species. Such distorted, or low symmetry, quadrupolar ^{27}Al sites are often broadened beyond detection, rendering them unobservable by NMR,[42,67] even under high field and fast spinning conditions. The increase in NMR visibility of ^{27}Al species in hydrated cement is consistent with the formation of more symmetric six-coordinate Al^{VI} sites, which experience inherently smaller quadrupolar interactions and the segregation of ^{27}Al species away from iron-containing components in the hydrated products. Quantitative ^{27}Al spin-counting analyses, thus, allow the fractions of ^{27}Al species in relatively ordered or disordered local environments to be estimated in anhydrous and hydrated cements.

Hydrated Aluminate Species in White Portland Cement. The molecular interactions between various ^{27}Al and ^{1}H species in white Portland cement that occur as a result of hydration can be monitored in detail by 2D ^{27}Al{^{1}H} HETCOR NMR measurements conducted at 11.7 T. Figure 7a shows the 2D ^{27}Al{^{1}H} HETCOR spectrum acquired using a very short ^{1}H spin-diffusion time of 10 μs to probe the immediate molecular proximities of different resolved ^{27}Al and ^{1}H species. Compared to the 1D single-pulse ^{1}H and ^{27}Al MAS spectra (Figure 7a, left and top), the intensity correlations observed in the 2D spectrum reveal specific and well-defined interactions between only a small subset of the components present. Specifically, a strong and narrow (1 ppm, fwhm) intensity correlation is observed between the ^{1}H signal at 1.2 ppm associated with hydroxyl species and the ^{27}Al signal at 9 ppm that is consistent with symmetric local environments of six-coordinate aluminum hydroxide moieties in ettringite (Figure 7a, inset). Weaker correlated intensity is also observed between the hydroxyl ^{1}H species at 1.2 ppm and the ^{27}Al signal at 5 ppm associated with hydrated aluminate thought to arise from six-coordinate TAH containing $Al(OH)_6^{3-}$ or $O_xAl(OH)_{6-x}^{(3+x)}$ moieties.[32] The 1D projections along the ^{1}H dimension show only one type of ^{1}H species corresponding to $-OH$ (1.2 ppm), while the signals from
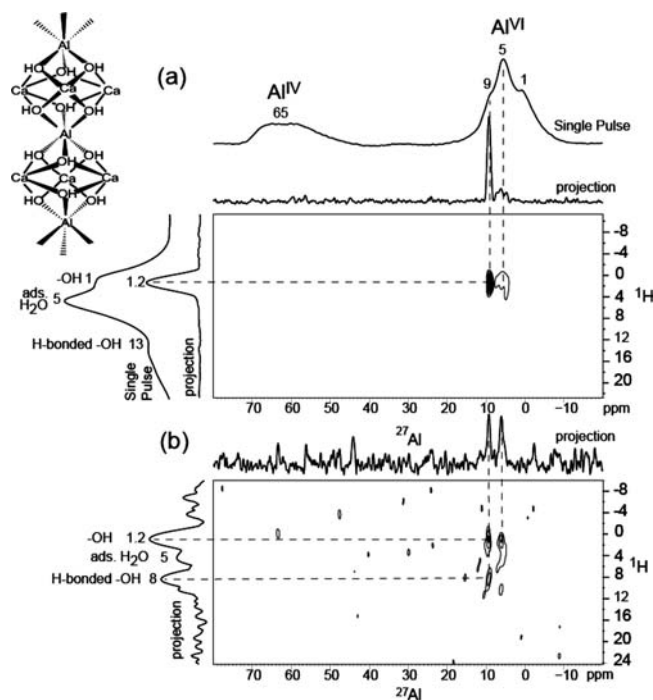

Figure 7. Solid-state 2D ^{27}Al{^{1}H} HETCOR NMR spectra acquired at 11.7 T at 278 K and 6.5 kHz MAS of hydrated white Portland cement with a 0.5 s recycle delay and different ^{1}H spin-diffusion times t_{sd} of (a) $t_{sd} = 10\ \mu$s and (b) $t_{sd} = 20$ ms. A 1D single-pulse ^{27}Al MAS spectrum is plotted along the top horizontal axis above a 1D ^{27}Al projection of the 2D spectrum. A 1D single-pulse ^{1}H MAS spectrum is plotted to the left of the 1D ^{1}H projection along the vertical axis. The lowest contour lines shown in the 2D spectra are 8% of maximum intensity. Inset: schematic diagram of the structure of ettringite to which the narrow ^{27}Al^{VI} signal at 9 ppm is assigned.

H_2O (5 ppm), and strongly hydrogen-bonded $-OH$ species (13 ppm) are absent. The absence of correlated signal intensity between ^{1}H species and four-coordinate ^{27}Al^{IV} moieties (ca. 65 ppm) indicates that the number of such dipole–dipole-coupled ^{1}H–^{27}Al^{IV} spin pairs is relatively small and/or that their mutual interactions are weak or broadly distributed. Moreover, the enhanced resolution of the 2D ^{29}Si{^{1}H} and ^{27}Al{^{1}H} HETCOR spectra in Figures 5 and 7 importantly allows ^{29}Si–OH (0.8 ppm ^{1}H) and ^{27}Al–OH (1.2 ppm ^{1}H) species to be distinguished. In combination, the 2D HETCOR spectra thus allow contributions from ^{1}H signals associated with the different hydration species, which otherwise strongly overlap and are unresolved in 1D ^{1}H spectra (Figure 7a, left), to be identified. The information contents and accompanying insights of the 2D HETCOR spectra are, therefore, significantly greater than can be obtained from separate 1D ^{1}H, ^{29}Si, or ^{27}Al MAS spectra, which yield no directly correlated information.

Note that the 2D ^{27}Al{^{1}H} HETCOR and accompanying 1D ^{27}Al MAS spectra in Figure 7 were recorded at 11.7 T, for which contributions from second-order quadrupolar interactions are expected to be greater than at 18.8 T (Figure 6). These lead to reduced resolution of the ^{27}Al signals present and modest changes in their peak positions in the single-pulse ^{27}Al MAS spectrum in Figure 7a. Another effect of the quadrupolar interaction is that the ^{27}Al signal rapidly decays during the contact time of the ^{27}Al–^{1}H cross-polarization experiment, and as a result, only those ^{27}Al sites that have relatively small quadrupolar coupling constants are observed in the 2D HETCOR spectra. Figure 7b shows the 2D ^{27}Al{^{1}H} HETCOR spectrum acquired using a ^{1}H spin-diffusion time of 30 ms to probe

(67) Shertukde, P. V.; Hall, W. K.; Dereppe, J. M.; Marcelin, G. *J. Catal.* **1993**, *139*, 468–481.

weaker molecular interactions between ^{27}Al and ^{1}H over longer distances (1−3 nm) or due to mobile ^{1}H moieties. Compared to the spectrum in Figure 7a, additional correlated signal intensity is observed between the ^{27}Al signal at 9 ppm and hydrogen-bonded −OH species resonating at 8 ppm in the ^{1}H dimension (although with diminished intensity, due to T_1 relaxation during the spin-diffusion time). The appearance of this intensity correlation indicates that these Al^{VI} species are in nanoscale proximity to adsorbed or hydrogen-bonded −OH species, likely either as part of hydrated aluminate components or adsorbed onto particle surfaces. The 2D $^{27}Al\{^{1}H\}$ HETCOR spectra thus reveal specific interactions between the ^{1}H and ^{27}Al moieties that have not previously been observed and show that highly symmetric Al^{VI}−OH species are predominant products of hydration at room temperature after 28 days.

Silicates and Aluminates in Gray Oilwell Cement

Anhydrous Gray Oilwell Cement: ^{29}Si NMR. Gray oilwell cements are manufactured by using similar raw materials and production processes as for white Portland cement, resulting in similar compositions and structures, although with several notable differences. As in white Portland cement, the anhydrous oilwell cement used in this study was also multicomponent, polycrystalline (Supporting Information, Figure S2a), and similarly composed (Table 1) principally of calcium silicate phases (84 wt %), with minor concentrations of aluminate (3.0 wt %) and sulfate (2.8 wt %). However, unlike white Portland cement, gray oilwell cements generally possess increased concentrations of metal oxide components, such as ferrite (Fe_2O_3, 4.3 wt %, Table 1) and MgO (3.3 wt %), or as ions that are present within the silicate or aluminate phases. Consequently, gray oilwell cements are more complicated mixtures with increased local structural disorder, whose individual molecular species and interactions are more challenging to investigate.

In particular for NMR studies, the presence of para/ferromagnetic iron-containing components in gray oilwell cements results in significantly shorter spin−lattice (T_1) relaxation times of nearby NMR-active species that can also result in a loss of NMR visibility, even for spin-1/2 ^{29}Si nuclei. For example, the 1D single-pulse ^{29}Si MAS spectrum of anhydrous gray oilwell cement in Figure 8a shows broad signal intensity between −66 and −77 ppm that can be fit to several overlapping Gaussian lineshapes, including signals centered at −71 and −73 ppm that are also present in the T_1-filtered (t_{T1} = 2 s) ^{29}Si MAS spectrum in Figure 8b. Compared to anhydrous white Portland cement (Figure 1) and despite the high crystallinity of the gray oilwell cement (Supporting Information., Figure S2a), the ^{29}Si MAS linewidths are much broader, and the overall signal intensity in the T_1-filtered spectrum (scaled by a factor of +16) is significantly lower. This is in spite of a shorter T_1-filter time that was used in Figure 8b (t_{T1} = 2 s), because of the faster T_1 relaxation of ^{29}Si moieties in the di- and tricalcium silicate phases of anhydrous gray oilwell cement, compared to the white Portland variety. Use of a longer filter time, e.g., t_{T1} = 10 s (as used in Figure 1), yielded a similar spectrum, but with even lower signal intensity.

Iron-containing components in anhydrous gray oilwell cement appear to be distributed nonuniformly, the effects of which are much more pronounced and significantly more complicated than for white Portland cements. Such differences in the proximities of silicate and iron-containing components can nevertheless be discerned by exploiting differences in ^{29}Si T_1 relaxation times
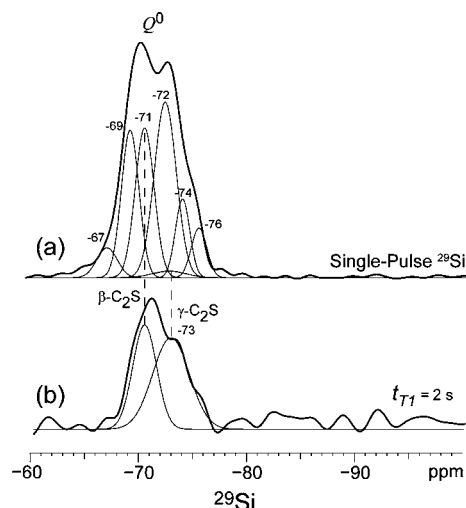

Figure 8. Solid-state 1D ^{29}Si MAS NMR spectra of anhydrous gray oilwell cement acquired at room temperature and 5 kHz MAS with a 10 s recycle delay and with different spin−lattice relaxation-time filters: (a) a single-pulse ^{29}Si MAS spectrum (t_{T1} = 0 s) and (b) with t_{T1} = 2 s, showing signals from different Q^0 ^{29}Si species associated with dicalcium silicate (β-, γ-C$_2$S). The spectrum in (b) has been scaled by a factor of +16, reflecting its much lower overall intensity.

to distinguish otherwise strongly overlapping ^{29}Si signals. This is achieved by using a combination of 1D T_1-filtered and saturation-recovery ^{29}Si MAS experiments, which allow ^{29}Si signals from silicate species in C$_2$S and even different C$_3$S phases to be observed and deconvoluted, based on their different spin−lattice relaxation behaviors. Such analyses (Figure 8 and Figure S5, Supporting Information) identify seven ^{29}Si signals in anhydrous gray cement, five of which at −67, −69, −72, −74, and −76 ppm are associated with ^{29}Si species that relax rapidly (<10 ms) and are attributed to different silicate species within the C$_3$S phases. (The ^{29}Si MAS spectra acquired with different ^{29}Si T_1-relaxation-time filters were each fit with the peak positions and linewidths constrained among the different spectra for each sample, see the Experimental Section and Figure S5, Supporting Information.) By comparison, the peaks at −71 and −73 ppm correspond to ^{29}Si signals that relax much more slowly (>2 s) and are assigned to β- and γ-C$_2$S, respectively. These results are consistent with previous studies of white Portland[36] and gray oilwell[28] cements, which reported multiple overlapping ^{29}Si MAS signals that reflect different ^{29}Si environments within different polymorphs of tricalcium silicate present in cements.

Consequently, the Q^0 ^{29}Si signals at −71 and −73 ppm in Figure 8b are attributed to β- and γ-C$_2$S, respectively, both signals of which are broadened by the presence of nearby para/ferromagnetic iron components. This is consistent with the much higher bulk concentration of Fe species in the anhydrous gray oilwell cement, which was ca. 12 times higher than for the white Portland cement examined (Table 1). The broad C$_2$S ^{29}Si signal at −71 ppm in Figure 8 and the significantly reduced T_1 relaxation times for all ^{29}Si species present in the gray oilwell cements indicates that iron species are associated with the C$_2$S, as well as the C$_3$S, phases. Indeed, ^{29}Si signals from silicate species in the C$_3$S phase(s) cannot be isolated from the C$_2$S polymorphs in a difference spectrum (as used for white Portland cement, Figure 1c) because the 2-s T_1 filter effectively suppresses the ^{29}Si signals from silicate species in both the C$_3$S and C$_2$S phases. However, the ^{29}Si signals from these species are distinguished on the basis of their T_1 relaxation times by using
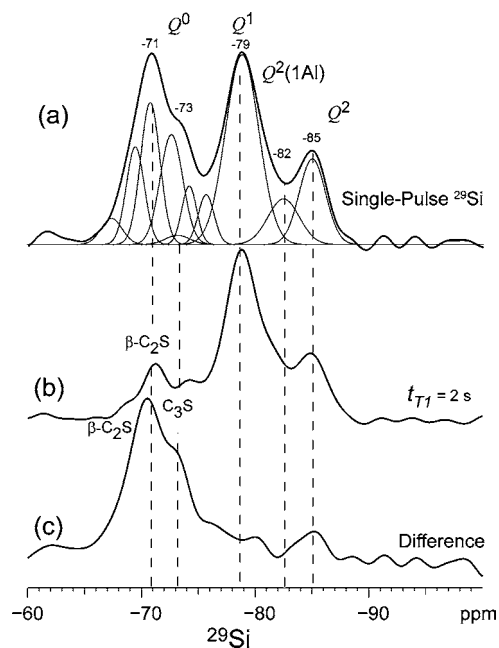
Figure 9. Solid-state 1D ^{29}Si MAS NMR spectra of hydrated gray oilwell cement acquired at room temperature and 5 kHz MAS with a 10 s recycle delay and different spin−lattice relaxation-time filters: (a) a single-pulse ^{29}Si MAS spectrum (t_{T1}= 0 s) showing ^{29}Si signals from partially condensed Q^1 and Q^2 ^{29}Si moieties associated with calcium-silicate-hydrate (CSH); (b) a T_1-filtered spectrum with t_{T1} = 2 s, which suppresses ^{29}Si signals from C$_3$S, yielding ^{29}Si signals from Q^0 species in C$_2$S and Q^1 and Q^2 moieties in CSH; and (c) the difference spectrum between (a) and (b), which resolves ^{29}Si signals from C$_3$S and fast-relaxing C$_2$S.

1D saturation recovery experiments (Supporting Information, Figure S5), where the significantly shorter T_1 values of the ^{29}Si species in C$_3$S and greatly reduced and broadened ^{29}Si signal intensities indicate the closer proximities of silicate moieties in C$_3$S to para/ferromagnetic Fe species, compared to the C$_2$S phases, including its relatively fast-relaxing ^{29}Si moieties. These results are consistent with previous X-ray analyses of crystalline phases in bulk gray cements,[68] with substantial additional molecular-level details provided by the NMR measurements.

Hydrated Gray Oilwell Cement: ^{29}Si NMR. Similar solid-state single-pulse and T_1-filtered ^{29}Si MAS NMR measurements allow the molecular changes that occur within the calcium silicate components during hydration of gray oilwell cement to be assessed and quantified. This includes also disordered products, which account for the reduced crystallinity of the hydrated cement (Supporting Information, Figure S2b). (The average bulk compressive strength of the gray oilwell cement used here was measured to be ca. 35 MPa following hydration at room temperature after 28 days.) As for hydrated white Portland cement (Figure 3), the 1D single-pulse ^{29}Si MAS spectrum shown in Figure 9a of hydrated gray oilwell cement exhibits significant signal intensity in the region −78 to −87 ppm, attributed to Q^1, Q^2, and Q^2(1Al) moieties in CSH. Also similarly, this is accompanied by a substantial reduction in the intensities of the signals between −67 and −76 ppm, consistent with the reaction of predominantly Q^0 ^{29}Si species in C$_3$S, which hydrate much more quickly than the C$_2$S phases. Figure 9b shows a 1D T_1-filtered ^{29}Si MAS spectrum (t_{T1} = 2 s) that exhibits signals from the anhydrous Q^0 ^{29}Si species at −71 and −73 ppm, which are suppressed relative to signals from the

(68) Hall, C.; Scrivener, K. L. *Adv. Cem. Based Mater.* **1998**, *7*, 28–38.
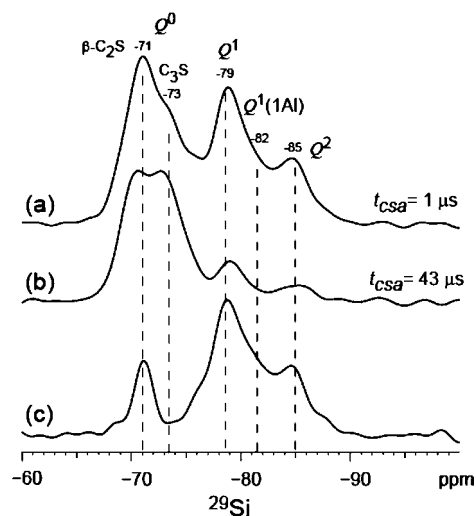
Figure 10. Solid-state 1D chemical-shift-anisotropy-filtered ^{29}Si MAS NMR spectra of hydrated gray oilwell cement acquired at room temperature and 5 kHz MAS with a 10 s recycle delay: (a) t_{csa} = 1 μs recoupling time, (b) t_{csa} = 43 μs recoupling time, and (c) a scaled difference spectrum between (a) and (b).

hydrated Q^1, Q^2(1Al), and Q^2 ^{29}Si moieties at −79, −82, and −85 ppm, respectively. These results are similar to those observed for hydrated white Portland cement (Figure 2). In addition, the changes in relative intensities associated with these hydrated ^{29}Si moieties in gray oilwell cement are consistent with segregation of the Fe species away from the disordered CSH products upon hydration. The Q^0 ^{29}Si signal at −71 ppm in Figure 9b remains much broader than that observed for hydrated white Portland cement (Figure 2b), as for the anhydrous material and are attributed mainly to unhydrated iron-containing C$_2$S. The scaled difference spectrum in Figure 9c (Figure 9b subtracted from Figure 9a) exhibits broad faster-relaxing ^{29}Si signals at −71 and −73 ppm from silicate species in C$_2$S and unreacted C$_3$S that are likely in close proximity to iron components. The solid-state single-pulse and T_1-filtered ^{29}Si spectra show that, aside from the resolution complications presented by the iron-containing components, gray oilwell cement appears to hydrate at a molecular level in a manner similar to white Portland cement. This includes the preferential segregation of Fe species associated with C$_3$S away from the CSH products formed during hydration. Given the very different molecular signatures of the respective ^{29}Si NMR spectra for the gray and white cements and the corresponding compositional and structural differences that they reflect, such similar molecular hydration behaviors are far from obvious.

Based on the T_1-filtered ^{29}Si MAS NMR results above, the ^{29}Si species in CSH appear to have similar ^{29}Si T_1 relaxation times, and therefore, as with white Portland cement, the individual signals cannot be resolved by using a T_1 filter alone. However, as shown in Figure 10, the application of a ^{29}Si CSA filter, as previously demonstrated for hydrated white Portland cement (Figure 3) also results in improved spectral resolution of signals from the various hydrated ^{29}Si species in gray oilwell cement. Compared to the CSA-filtered spectrum of hydrated gray oilwell cement acquired with a very short filter time t_{CSA} = 1 μs (Figure 10a), a longer time t_{CSA} = 43 μs (Figure 10b) significantly suppresses the signals from Q^1, Q^2(1Al), and Q^2, species at −79, −82, and −85 ppm, respectively, from the CSH product, compared to the Q^0 ^{29}Si signals at −71 and −73 ppm. As shown in Figure 10c, however, the scaled difference

Table 4. Relative Site Populations of NMR-Visible ^{29}Si Species in the Anhydrous and Hydrated Gray Oilwell Cements Used in This Study

anhydrous gray oilwell cement			hydrated gray oilwell cement		
assignment	^{29}Si signal (ppm)	relative % of visible ^{29}Si	assignment	^{29}Si signal (ppm)	relative % of visible ^{29}Si
Q^0, β-C$_2$S	−71	21 (±3)	Q^0, β-C$_2$S	−71	15 (±3)
Q^0, C$_3$S	−67 to −76	79 (±3)	Q^0, C$_3$S	−67 to −76	30 (±3)
			Q^1	−79	36 (±2)
			Q^2(1Al)	−81	7 (±2)
			Q^2	−85	12 (±2)

spectrum reveals less resolution enhancement among the Q^1, Q^2(1Al), and Q^2 ^{29}Si signals than achieved for hydrated white Portland cement (Figure 3). It is interesting to note that the ^{29}Si signal at −71 ppm from the Q^0 ^{29}Si species in β-C$_2$S is dephased to a significantly greater extent in the hydrated gray oilwell cement, thus reflecting a significantly larger ^{29}Si CSA, compared to the other Q^0 species in the calcium silicate phases. This reflects local bonding environments of ^{29}Si sites in the β-C$_2$S phase of the gray oilwell cement that are different from those of the γ-C$_2$S phase and are also different from those of both the β-C$_2$S and γ-C$_2$S phases of the white Portland cement analyzed above. The origins of these differences remain under investigation, but may be due to a greater extent of cation substitution in the β-C$_2$S phase of this gray oilwell cement. These results confirm the sensitivity of the ^{29}Si CSA- and T_1-filters to local compositional and structural features of cements that distinguish subtle differences among precursor and product cement species.

Quantification of ^{29}Si Species in Anhydrous and Hydrated Gray Oilwell Cements. Although the iron-containing components and associated broadening of ^{29}Si NMR signals in anhydrous and hydrated gray oilwell cements can make the identification and quantification of ^{29}Si species difficult, by deconvoluting, integrating, and comparing the relative areas of the ^{29}Si lineshape fits, insights into the hydration process can nevertheless be obtained. From comparison of quantitative single-pulse ^{29}Si MAS NMR spin-counting measurements and elemental analyses, 98% of ^{29}Si species are visible in the anhydrous gray oilwell cement. Though exhibiting significantly broadened ^{29}Si signals, due to the proximity of para/ferromagnetic iron-containing components, nearly all ^{29}Si species are detected. Using saturation-recovery ^{29}Si MAS analyses, the overlapping ^{29}Si signals from different silicate species in the anhydrous gray cement can be distinguished and their relative populations estimated. The relative concentrations of different silicate species are determined by integrating Gaussian lineshape fits to the overlapping signals in the quantitative single-pulse ^{29}Si MAS spectrum of Figure 8a. These fits are based on the resolved lineshapes in the Supporting Information, Figure S5, which increase the confidence of the analyses that yield the relative concentrations of the different silicate species tabulated in Table 4 (center). The ^{29}Si Q^0 signal at −71 ppm associated with β-C$_2$S accounts for 21% of the overall ^{29}Si intensity, while the remaining 79% of the total ^{29}Si signal arises predominantly from C$_3$S, including minor contributions (∼1%) from γ-C$_2$S. Furthermore, it is interesting to note in Figure 8b that the weak ^{29}Si intensity at −73 ppm attributed to γ-C$_2$S is significantly more intense relative to the ^{29}Si signal at −71 ppm of the β-C$_2$S, compared to those observed for white Portland cement (Figure 2b). ^{29}Si spin-counting measurements establish that the absolute quantities of silicate species in γ-C$_2$S are comparable in both the gray and white cements, indicating that the ^{29}Si signals from

silicate species in the β-C$_2$S phase in the gray cement are significantly more suppressed by the 2-s T_1 filter. These results suggest a significantly higher concentration of Fe species in the β-C$_2$S polymorph, compared to γ-C$_2$S in the gray cement. The use of solid-state single-pulse, T_1-filtered, and saturation-recovery ^{29}Si MAS NMR thus allows the β-C$_2$S and γ-C$_2$S dicalcium silicate and C$_3$S tricalcium silicate phases to be identified and quantified and the proximities of para/ferromagnetic iron species to be established for the siliceous components of anhydrous gray oilwell cement.

As with white Portland cement, the uses of ^{29}Si T_1 and CSA filters allow the ^{29}Si signals and lineshapes of Q^1, Q^2, and Q^2(1Al) silicate species in the hydrated gray oilwell cement to be distinguished, enabling their relative populations to be estimated, as summarized in Table 4. Quantitative single-pulse ^{29}Si MAS NMR spin-counting measurements and elemental analyses confirm that all of the ^{29}Si species in the hydrated gray oilwell cement are visible. The relative concentrations of the Q^0 species in C$_2$S and C$_3$S were estimated using the same ^{29}Si peak positions as determined for anhydrous gray oilwell cement. As for anhydrous white Portland cement discussed above, the C$_3$S/C$_2$S ratio in anhydrous gray oilwell cement is calculated by quantitative ^{29}Si NMR lineshape analysis to be 3.8 (±0.7), in excellent agreement with the ratio calculated by Rietveld analysis of the XRD patterns for which a value of 3.8 (±0.4) is independently obtained (Supporting Information, Figure S2a and Table S2). The concentration of visible Q^0 species relative to the Q^1, Q^2, and Q^2(1Al) species in the hydrated gray oilwell cement is determined to be 45%, which is similar to that for white Portland cement hydrated under equivalent conditions (47% ^{29}Si Q^0 species). Of these, the ^{29}Si Q^0 signal at approximately −71 ppm associated with the dicalcium silicate phases corresponds to 15% of the total ^{29}Si signal intensity in Figure 9a, reduced from 21% in the anhydrous cement (Figure 8a). Compared to white Portland cement (where C$_2$S reacts negligibly, Figure 2a), the apparently enhanced reactivity of the silicate species in β-C$_2$S may result from increased ion substitutions, such as Fe^{3+}. The ^{29}Si Q^0 moieties associated with the tricalcium silicate phases (−67 to −76 ppm) account for 30% of the signal intensity (Figure 9a), compared to 79% in the anhydrous starting material (Figure 8a), again consistent with faster hydration kinetics compared to the dicalcium silicates. Integration of the lineshape fits to the ^{29}Si signals at −79, −82, and −85 ppm establish the approximate mole percents of the cross-linked Q^1, Q^2(1Al), and Q^2 ^{29}Si moieties to be 36%, 7%, and 12%, respectively, in the CSH. The relative ratios of the Q^1, Q^2(1Al), and Q^2 ^{29}Si species in both the hydrated gray oilwell and white Portland cements are nearly identical, indicating similar hydration processes and kinetics in the different cements.

Anhydrous and Hydrated Gray Oilwell Cement: ^{27}Al NMR. Similar changes in aluminate species within gray oilwell cement during hydration can be monitored by using solid-state ^{27}Al MAS NMR at very high magnetic field strengths to resolve signals from a variety of aluminate species.[35] For example, the 1D single-pulse ^{27}Al MAS spectra of anhydrous and hydrated gray oilwell cements recorded at 18.8 T are shown in Figure 11a,b, respectively. For anhydrous gray oilwell cement, several ^{27}Al signals are observed that can be assigned to similar aluminate components as found in anhydrous white Portland cement (Figure 6a):[4,5,30,62,63] 80 and 86 ppm, corresponding to ^{27}Al^{IV} moieties in the C$_2$S and C$_3$S phases, respectively; 20 ppm associated with ^{27}Al^{VI} species in aluminate grain-boundaries;
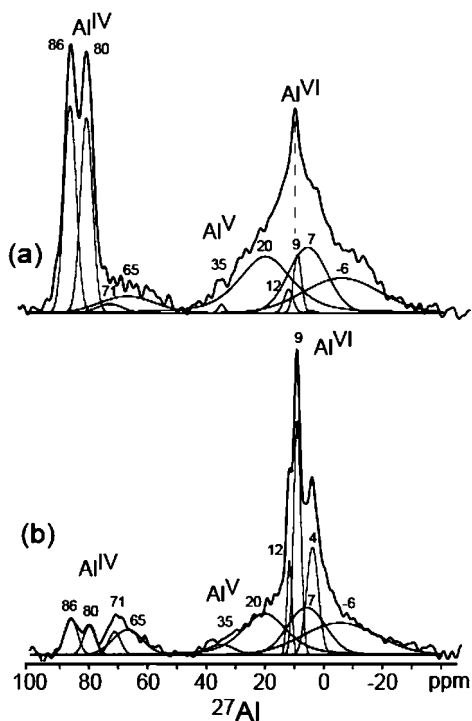
Figure 11. Solid-state 1D single-pulse ^{27}Al MAS NMR spectra acquired at 18.8 T at room temperature and 20 kHz MAS for (a) anhydrous and (b) hydrated gray oilwell cements. Deconvolution fits to the spectra are shown, along with their respective peak positions.

Table 5. Relative Site Populations of NMR-Visible ^{27}Al Species in the Anhydrous and Hydrated Gray Oilwell Cements Used in This Study

anhydrous gray oilwell cement			hydrated gray oilwell cement		
assignment	^{27}Al signal (ppm)	relative % of visible ^{27}Al	assignment	^{27}Al signal (ppm)	relative % of visible ^{27}Al
Al^{IV}	86	16 (±2)	Al^{IV}	86	4 (±2)
Al^{IV}	80	15 (±3)	Al^{IV}	80	3 (±1)
Al^{IV}	71	2 (±1)	Al^{IV}	71	2 (±1)
Al^{IV}	65	6 (±2)	Al^{IV}	65	6 (±3)
Al^{V}	35	1 (±1)	Al^{V}	35	2 (±1)
Al^{VI}	20	22 (±5)	Al^{VI}	20	18 (±3)
Al^{VI}	12	2 (±1)	Al^{VI}	12	4 (±2)
Al^{VI}	9	3 (±2)	Al^{VI}	9	14 (±1)
Al^{VI}	7	17 (±5)	Al^{VI}	7	16 (±5)
Al^{VI}	4	<1 (±1)	Al^{VI}	4	11 (±3)
Al^{VI}	−6	16 (±3)	Al^{VI}	−6	20 (±4)

increased. These results are consistent with similar observations made for the anhydrous and hydrated white Portland cements discussed above (Figure 6.)

Quantification of ^{27}Al Species in White Portland Cement. The reduced ^{27}Al MAS linewidths and increased sensitivity of the ^{27}Al MAS spectra (Figure 11) acquired at 18.8 T yield significantly enhanced resolution of signals from different Al-containing components in gray oilwell cements than have previously been observed. This results in both improved identification and quantification of distinct NMR-visible Al^{IV}, Al^{V}, and Al^{VI} species that, until now, have not been resolved in ^{27}Al NMR spectra of gray oilwell cements. As a result, the ^{27}Al MAS spectra of the anhydrous and hydrated gray oilwell cements in Figure 11a,b can be fit and deconvoluted by using Gaussian lineshapes (Supporting Information, Figure S6), whose integrated peak areas allow the relative site populations of the different NMR-visible ^{27}Al species to be estimated, as listed in Table 5. Broad and overlapping ^{27}Al signals, such as those associated with Al^{VI} species at −6, 7, and 20 ppm, are of course difficult to deconvolute with certainty, so that the resulting analyses cannot be considered unique and must therefore be interpreted with caution. Nevertheless, estimates of the relative concentrations of ^{27}Al NMR-visible species are useful, especially when the lineshape analyses have been fit, deconvoluted, and compared among closely related samples, as the case for the cement samples examined here.

Consequently, ^{27}Al MAS lineshape analyses (Figure 11a,b) and the relative integrated signal intensities associated with NMR-visible ^{27}Al species in anhydrous and hydrated gray oilwell and white Portland cements can be compared and contrasted. Specifically, Al^{V} and Al^{VI} species account for 61% of the ^{27}Al NMR-visible species in "anhydrous" gray oilwell cement, while the remaining 39% of visible ^{27}Al species are Al^{IV} moieties (present in C_3A, C_4AF, C_2S, and C_3S). Importantly, quantitative single-pulse spin-counting ^{27}Al MAS NMR measurements (not shown here) establish that in the case of anhydrous gray oilwell cement, only 10% of the aluminate species are visible by ^{27}Al NMR, compared to 20% for anhydrous white Portland cement. There is also increased NMR visibility of more symmetric six-coordinate $^{27}Al^{VI}$ sites and ^{27}Al species segregated from iron-containing components in the oilwell cement. By comparison, the relative concentration of visible Al^{V}, and Al^{VI} species increases from 61% in anhydrous gray oilwell cement to 85% upon hydration, while the anhydrous Al^{IV} species are correspondingly reduced from 39% to 15%. Interestingly, the $^{27}Al^{IV}$ broad signal at ca. 65−71 ppm associated with the C_3A and C_4AF species in anhydrous gray

12 ppm associated with $^{27}Al^{VI}$ species in ettringite (formed as a result of hydration during storage); and the broad underlying signal centered at ca. 7 ppm associated with $^{27}Al^{VI}$ species in CSH and/or aluminoferrite (C_4AF). The ^{27}Al signals at ca. 65−71 ppm attributed to Al^{IV} sites in C_3A and C_4AF are much less intense in the anhydrous oilwell cement, compared to anhydrous white Portland cement. This is likely due to the significantly higher concentration of Fe species in the gray cement, which based on this observation, indicates that a principal source of Fe^{3+} species appears to be the C_4AF phase, consistent with para/ferromagnetic broadening of its ^{27}Al signals beyond detection. Weak signal intensity is also observed at ca. 35 ppm associated with partially hydrated $^{27}Al^{V}$ moieties in CSH, along with additional signals that are not observed in anhydrous white Portland cement: hydrated monosulfate (9 ppm) and additional aluminate hydrates associated with broad ^{27}Al signal intensity centered at ca. −6 ppm. This indicates a greater extent of hydration for the "anhydrous" gray oilwell cement, compared to anhydrous white Portland cement, which likely occurs during storage and is possibly augmented by the higher iron contents of the gray oilwell cement.

The 1D single-pulse ^{27}Al MAS spectrum of hydrated gray oilwell cement shown in Figure 11b exhibits features similar to those observed for hydrated white Portland cement (Figure 6b). Compared to the respective anhydrous material, the overall intensities of the $^{27}Al^{IV}$ signals (Figure 11b) are significantly reduced, with evidence of unreacted aluminosilicate species in C_2S and C_3S remaining (80 and 86 ppm). More intense $^{27}Al^{VI}$ signals are observed from the hydration products ettringite (12 ppm), monosulfate (9 ppm), and TAH (4 ppm). The broad ^{27}Al signals at 20 and 7 ppm assigned to Al^{VI} moieties in aluminate grain-boundary phases and in CSH or aluminoferrite, respectively, appear with reduced intensity, while the broad ^{27}Al signal attributed to hydrated aluminate species at −6 ppm has

oilwell cement appears to increase somewhat in intensity with hydration, which may reflect intensity contributions from Al^{IV} species in disordered CSH.

Quantitative single-pulse spin-counting ^{27}Al MAS NMR measurements separately establish that in the case of hydrated gray oilwell cement, only 20% of the aluminate species are visible by ^{27}Al NMR. While this is approximately twice the quantity of visible species as determined for anhydrous gray oilwell cement, it is much less than the 80% visible in hydrated white Portland cement and indicates that a large fraction of the aluminate species remain unaccounted for by ^{27}Al NMR, even at the very high magnetic field strength (18.8 T) used here. The presence of iron in the gray oilwell cements suppresses NMR signals of nearby ^{27}Al species, due to para/ferromagnetic effects and may also induce local compositional and structural disorder near Al species that exacerbate quadrupolar broadening of the ^{27}Al signals. This indicates that a significant portion of the aluminate species remain closely associated with iron and undetectable in the ^{27}Al NMR spectra. The visibility and linewidths of ^{29}Si and ^{27}Al MAS NMR signals from the different silicate and aluminate components in cements, nevertheless, provide insights into the proximities and concentrations of iron species in the different components and associated changes during hydration. This sensitivity demonstrates the utility of ^{29}Si and ^{27}Al NMR for monitoring the early hydration processes in both white Portland and gray oilwell cements, including when Fe species are present.

Conclusions

The relative concentrations, molecular structures, and interactions of different components in the anhydrous and hydrated white Portland and gray oilwell cements have been assessed by solid-state NMR spectroscopy to understand and compare their molecular-level properties. The uses of complementary NMR methodologies yield high resolution ^{29}Si and ^{27}Al spectra that allow different silicate and aluminate species to be distinguished and quantified. Solid-state 1D single-pulse ^{29}Si and ^{27}Al MAS spectra, T_1- or CSA-filtered ^{29}Si MAS spectra, and 2D $^{29}Si\{^1H\}$ and $^{27}Al\{^1H\}$ HETCOR NMR spectra of hydrated white Portland cement reveal detailed molecular interactions of various hydrogen-containing species with silicate and aluminate species, yielding new insights on local compositions and structures of products that are formed during cement hydration processes. Heterogeneous distributions of hydroxyl species and strongly adsorbed water are observed in calcium-silicate-hydrate and hydrated aluminate products that correlate to different ^{29}Si and ^{27}Al sites produced during cement setting. The role of iron is complicated as to its influences on cement composition and hydration and challenging with respect to the effectiveness of bulk scattering and molecular NMR investigations. However, T_1-, CSA-filtered, and saturation-recovery ^{29}Si measurements can exploit the heightened spin-relaxation and broadening effects associated with para/ferromagnetic Fe species in cement to identify components with differing iron concentrations. In white Portland cement, iron-containing species are observed to segregate from C_3S phases during the formation of hydration products (CSH). Aluminate (C_3A) phases rapidly form ettringite in white Portland cement, while gray oilwell is observed to form additional hydrated aluminates that partially separate from iron as well. Despite the presence of higher iron levels in gray oilwell cements and reduced NMR signal visibilities of certain species, the fundamental hydration processes and resulting local compositions and structures appear to be similar to white Portland cements. The use of very high magnetic fields provides significant NMR sensitivity and resolution enhancements, especially for quadrupolar ^{27}Al aluminate species. Work is currently underway in our laboratories to develop and further apply advanced NMR techniques to establish transient evolution behaviors of these silicate and aluminate components and resulting products of the hydration process.

Supporting Information Available: Powder X-ray diffraction patterns, scanning electron micrographs, Gaussian lineshape fits and peak deconvolutions for the experimental solid-state 1D single-pulse ^{27}Al and ^{29}Si MAS NMR spectra. This material is available free of charge via the Internet at http://pubs.acs.org.

JA908146M